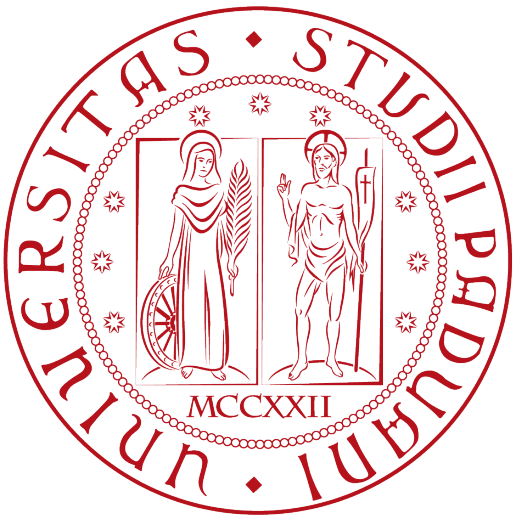

Università degli Studi di Padova
Dipartimento di Fisica ed Astronomia "G. Galilei"

Tesi di Laurea Magistrale in Fisica

Statistics of Living Polymer Rings

Laureando:
Luigi Gattone

Relatore:
Prof. Enzo Orlandini

Anno Accademico 2015/2016

Contents

Chapter 1

Introduction

A polymer i a macromolecule composed of many repeated subunits. Polymers range from synthetic plastics such as polystyrene to natural biopolymers such as DNA and proteins; because of their broad range of properties, such as elasticity, tensile strenght and diffusivity, both synthetic and natural polymers play an important role in everyday life.
The entire structure of a polymer is created during polymerization, which is the process that binds together elementary units, knows as monomers. The chemical identity of monomers and the polymer's microstructure are two of the major factors determining the properties of polymerics systems. However we are interested in another important feature controlling the properties of this kind of systems, which is the polymer architecture. Types of polymer architectures include linear, ring, star-branched, H-brenched, comb, ladder, dendrimer or randomly branched. [1]
A particular class of polymers are the so called living polymers.Living polymers are macromolecules that can break and recombine on experimental time scales. For example, an ensamble of DNA fragments, in presence of recombinase, can separate and rejoin in different manners. Recombenase are site-specific enzymes that are responsible for processes such as viral infections [2].
We focus our attention on polymer rings, in particular we want to study the effect of spatial confinement on their dynamical and metric properties at equilibrium. In order to do that we are going to use a coarse-grained model of circular polymers described as closed chain of beads hosted in a solved at a given temperature T. We will perform numerical analysis on confined systems with fixed number of monomers, but variable number of polymers.
In particular we are going to focus our attention to the effect of confinement on the polymers' radius of gyration and on the dynamic of their center of mass. The radius of gyration describes the polymers' estensivity, while the dynamic of the center of mass gives us information about their diffusivity properties.
Why are we interested in confined polymers? For example, a polymer subject to a strong geometrical constraint can reach an entangled state. The entanglemnt not only severely affects the physical properties of the indivitual polymer, but also of polymer melts. Moreover entanglement can be trapped during the crystallization of artificial polymers, affecting the properties of the resulting crystal such as its degree of purity. [3].
Another example of confined polymers is the case of biomolecules : DNA and RNA. The genomic material is subject to a very high degree of confinement: in eukaryotic cells DNA molecules with a contour length as large as $\sim 1m$ are packed in nucleus of the diameter of about $1\mu m$.

However the living cells that show the highest degree of DNA confinement are the so called Bacteriophages, which are viruses that infect bacteria. The DNAn typically double stranded, of these viruses is enclosed in a proteic stucture called capsid. The confinement inside the capsid affects the topology of the DNA, playing a key role in setting and controlling the ejection of the DNA during the infection of a bacteria [4].
Afer describing the effect of confinement, we are going to study how the polymer rings behave when they are given the possibility to swap bonds. This is exactly the case of enzymes such as recombenase acting on DNA molecules during process like cellular infection. In chapter two we introduce and describe the system properties, such as the polymers structure and the statistical ensamble in which they are contained, and we study the metric features and dynamic of a single isolated ring. In chapter three we still focus our attention on a single isolated ring, but with the addition of an external constraint which simulates the effect of confinement. In chapter four the work done in the previous chapters is extended on a solution of several rings, in order to describe how the mutual interaction between different polymers changes their dynamic and metric properties. Finally in chapter five we are going to divert our attention to solutions of living polymer rings, describing how the distribution of rings' lenght changes over time as function of monomere density.

Chapter 2

Model and numerical implementation

In order to perform a correct analysis is vital to define all the quantities and factors playing a crucial role in the dynamics of the polymer rings, such as the surrounding environment, bond types and pair interaction between non bonded atoms.

2.1 Description of the system

In this section we are going to exhibit all the features of the system taken into exam and the model we are going to perform our studies. We facilitate the investigation of ring polymer properties by using a coarse graining approach. In this metodology each monomer is substituted by a single-particle interacting with the others through carefully chosen potentials. Morover we are going to use particular types of polymers, called homopolymers, which are composed by only one type of monomer.

2.1.1 Bond type

The connectivity of the polymer chains is described by the finitely extensible nonlinear elastic potential (abbreviated FENE) [5].

$$U_{FENE} = \begin{cases} -\frac{1}{2}kr_0^2 ln[1-(r/r_0)^2] & r \leq r_0 \\ \infty & r > r_0 \end{cases} \tag{2.1}$$

where r_0 is a finite extensibility and k is a constant that has the dimension of energy over surface. The FENE potential is harmonic at its minimum but the bonds cannot be stretched beyond a maximum length determined by r_0. This potential alone is not sufficient to describe a polymer, beacaus it would allow neighbour beads to overlay. This problem is solved by introducing a Lennard-Jones type potential, described in the next section.

2.1.2 Pair interaction

Once defined the bond potential, is importand to chose wisely a pair interaction that grants self-avoidance among beads of the same chain and between different rings. A mathematically simple potential that approximate excluded volume interaction is the Lennard-Jones potential

$$V_{LJ} = 4\epsilon \left[\left(\frac{\sigma}{r}\right)^{12} - \left(\frac{\sigma}{r}\right)^{6} \right] \tag{2.2}$$

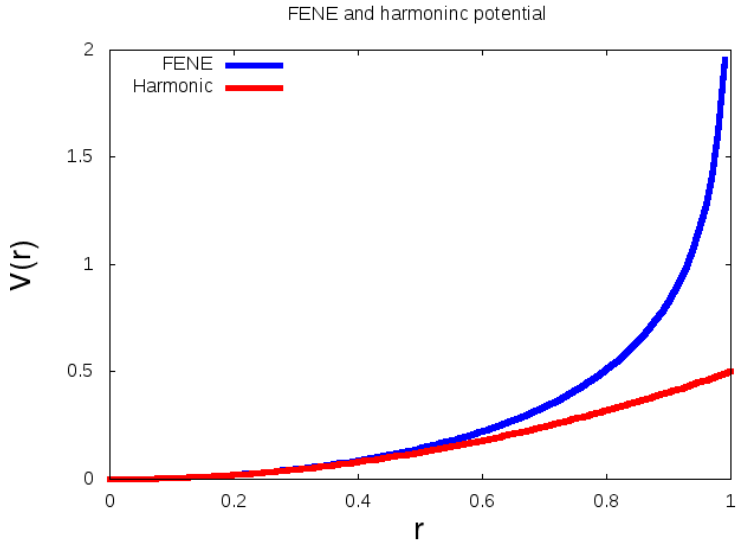

Figure 2.1: Comparison between FENE and harmonic potential with $r_0 = 1$ and $k = 1$

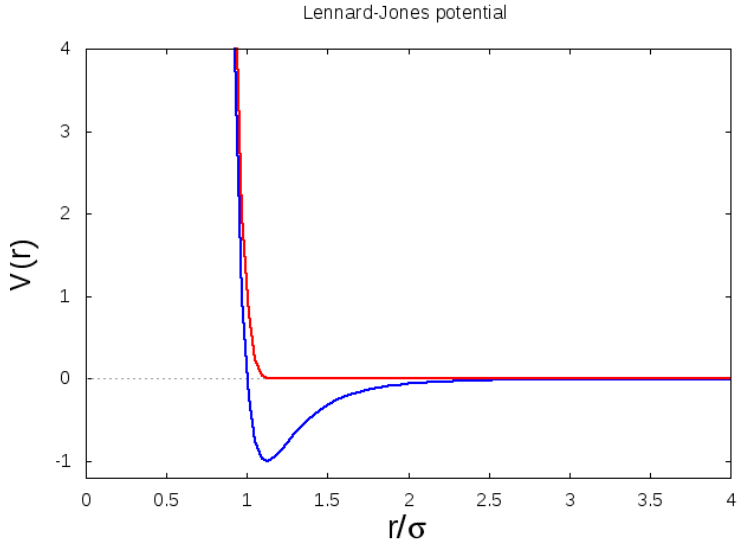

Figure 2.2: Standard and edited version of the LJ potential with $\epsilon = 1$

where ϵ is the depth of the potential well, σ is the finite distance at which the inter-particle potenzial is *zero* and r is the distance between the particles. At r_m the potential function has the values $-\epsilon$. The distance are related as $r_m = 1.122\sigma$. The advantage of the Lennard-Jones potential lies in its computational simplicity. The r^{-12} term describes Pauli repulsion at short ranges due to overlapping electron orbitals, r^{-6} term describes attraction at long ranges (van der Waals force, or dispersion force). However, since we describe the attractive interaction between consecutive beads by means of the FENE potential, we will use a modified version of the Lennard-Jones potential which introduces only a repulsive component. In order to do this we cut off the potential at its minumun and shifted it upwards. The explicit formula for this

version of the potential is :

$$V'_{LJ} = 4\epsilon \left[\left(\frac{\sigma}{r}\right)^{12} - \left(\frac{\sigma}{r}\right)^{6} + \frac{1}{4} \right] \theta(\sigma - r) \tag{2.3}$$

Together with the FENE potential we completed the description of the potentials affecting the system.

The introduction of the Lennard-Jones potential, gives the opportunity to rescale the physical units and to express every quantity as multiples of mass, σ,ϵ and k_B [6].

Quantity	Reduced form
Length	$r^* = r/\sigma$
Time	$t^* = t\left(\frac{\epsilon}{m\sigma^2}\right)^{1/2}$
Temperature	$T^* = K_B T/\epsilon$
Force	$F^* = F\sigma/\epsilon$
Energy	$E^* = E/\epsilon$
Pressure	$P^* = P\sigma^3/\epsilon$

Table 2.1: In this table are listed the physical units rescaled by means of the LJ potential. In this work, unless explicitly specified otherwise, we will always use this set of units.

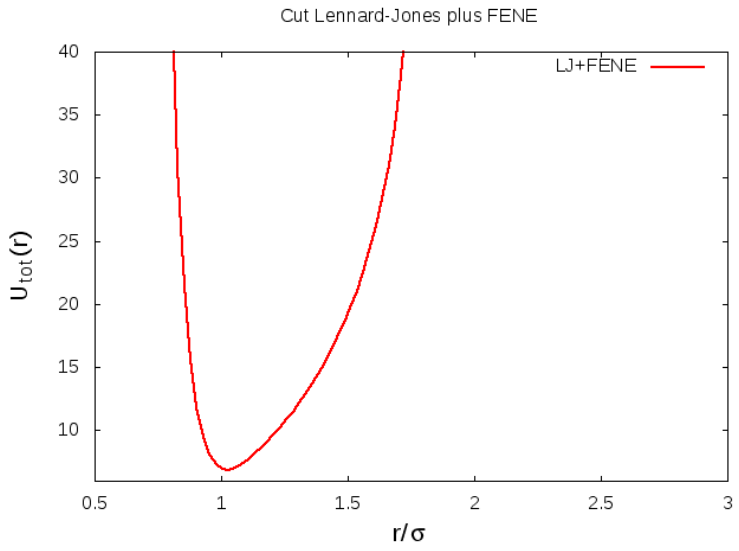

Figure 2.3: In this plot is shown the total potential interaction present in the system. Its the sum of FENE and cut-Lennard-Jones potential. Making this plot we used the actual quantity used during the simulation, in particular we set $\sigma = 1$, $r_0 = 1.8$ and $k = 10$

2.1.3 Dynamic of the system

In this section we focus our attention to the forces acting on the polymers. First of all we consider the conservative force $\vec{F}_c$ that comes from the inter-particle interaction; its explicit form is obteined computing the gradient of the total potential energy :

$$\begin{aligned}\vec{F_c} = -\boldsymbol{\nabla} U_{tot} = -\boldsymbol{\nabla}(U_{FENE}(r) + V'_{LJ}(r)) = -\frac{d}{dr}(U_{FENE}(r) + +V'_{LJ}(r))\hat{r} = \\ = \frac{r_0 r}{1 - r^2/r_0^2}\hat{r} + 4\epsilon\left[12\left(\frac{\sigma^{12}}{r^{13}}\right) - 6\left(\frac{\sigma^6}{r^7}\right)\right]\theta(\sigma - r)\hat{r} + \epsilon\delta(\sigma - r)\hat{r}\end{aligned} \tag{2.4}$$

Secondly, we suppose that the rings are in contact with a thermostat, which models an interaction with a background implicit solvent, at a given temperature T. This system is assumed to be isolated, it cannot exchange energy or particles with the environment, so that the energy of the system remains exactly known at every time. This ensamble is often referred to as NVE ensamble because number of particle N, the total energy in the system E and the system's volume V are microscopic variables that remain constant. The presence of the solvent naturally introduces the presence of a stochastic force which satisfies the Langevin equation

$$m_i \ddot{\vec{r_i}} = -\frac{m_i}{\xi}\dot{\vec{r_1}} + \vec{\eta} \tag{2.5}$$

This equation combines two different terms. The first one, which we call $\vec{F_f} = -\frac{m_i}{\xi}\dot{\vec{r}} = -\frac{m_i}{\xi}\vec{v}$, is a frictional drag or viscous damping tem proportional to the particle velocity. The proportionality constant for each atom is computed as $\frac{m_i}{\xi}$, where m_i is the mass of the particle and ξ is the friction; in this particular case we assume $m_i = m = 1$.

The second term, $\vec{\eta}$, is a force due to solvent atoms at a temperature T randomly bumping into the particle; As derived from the fluctuation/dissipation theorem, its magnitude is proportional to $\sqrt{\frac{k_B T m}{\xi \cdot dt}}$, where K_B is the Boltzmann constant, T is the desired temperature, m is the mass of the particle, dt is the timestep size, and ξ is, again, the friction. It has the statistical property of the so called white noise, which is described by the relations:

$$\langle \eta_\alpha(\vec{r}) = 0 \rangle \quad \text{and} \quad \eta_\alpha(\vec{r})\eta_\beta(\vec{r'}) = \sigma\delta_{\alpha\beta}\delta(\vec{r} - \vec{r'}) \tag{2.6}$$

In order to solve this system of Langevin equation we use a velocity-Verlet integration method, which is already built inside LAMMPS libraries. The parameters used during the simulations, for the Langevin dynamics, are: temperature $T = 1.0$ and friction $\xi = 0.5$, expressed in Lennard-Jones units.

2.2 Simulation and numerical analysis

The goal of this analysis is to describe how an ensamble of polymer rings, under confinement at different concentration, reaches an equilibrium state, that we characterize by computing some quantities. Initially we run several simulations in order to understand the basic behaviour of polymers. In doing so we will performe different simulation in a volume filled with rings of the same length, watching how number of rings N_R and the total number of monomers N affect the spatial arrangement. Also, is possible to change the volume in which the rings a conteined: we shall use a cubic box with periodic boundaries conditions ($V = 100x100x100$)and a sphere with hard walls.

First of all it is important to determine the density of polymers in the volume. A possible way of doing so, is to compute the volume fraction

$$\Phi = \frac{V_{rings}^{tot}}{V_{sys}^{tot}} = \frac{N_R V_{ring}}{V_{sys}^{tot}} \tag{2.7}$$

where N_R is the number of rings,V_{sys}^{tot} is the total volume of the system and V_{rings} is the volume of one ring. We suppose that one monomere occupies a spherical volum of diameter σ, therefore we get :

$$\Phi = N_R \frac{N\frac{4}{3}\pi(\frac{\sigma}{2})^3}{V_{sys}^{tot}} \tag{2.8}$$

We will, as said before, work with two types of geometries: a closed sphere and a periodic cubic box. This means that Φ has two formally distinct expressions:

$$\Phi_{box} = N_R \frac{N\frac{4}{3}\pi(\frac{\sigma}{2})^3}{L^3}, \tag{2.9}$$

$$\Phi_{sphere} = N_R \frac{N(\frac{\sigma}{2})^3}{R^3}, \tag{2.10}$$

where both L^3 and R^3 are multiples of σ^3, which means that Φ, being a number, does not depend on σ, as expected, since is adimensional. A typical quantity that measure the average extension of a polymer is the mean squared radius of gyration. Its importance is due to the fact that it can be estimated experimentally in many ways such as x-ray scatteringand static light scattering. [1]
The radius of gyration is defined as follows :

$$R_g^2 = \frac{1}{M}\sum_{i=1}^{N} m_i \left(r_i - R_{cm}\right)^2$$

where M is the total mass of the polymer, R_{cm} is its the center-of-mass position, and the sum is over all the monomers. We have already specified that the monomers have all the same unitary mass,hence the radius of gyration becomes:

$$R_g^2 = \frac{1}{N}\sum_{i=1}^{N} \left(r_i - R_{cm}\right)^2 \tag{2.11}$$

To study the motion of the rings we consider the center of mass. More specifically we compute $\Delta = \left\langle (\vec{r}_{CM}(0) - \vec{r}_{CM}(t))^2 \right\rangle = D\tau$, which is the mean squared displacement (MSD) of the center of mass' position. Assuming a diffusive motion of a single ring we can find the time at which the ring has travelled a distance equal to its own radius :

$$2dD\tau_{BD}^{ring} = R_g^2 \tag{2.12}$$

where $d = 3$ is the dimension of the system and D is the diffusion coefficient.This is roughly gives the time when the ring loses memory of itself. This means that after a time equal to τ_{BD}^{ring} the ring can be considered independent from the one we were observing before. With the symbol $\langle\cdot\rangle$ we denote the mean computed over various simulations with different initial conditions. A

possible way of describing the diffusion coefficient of the center of mass is through the Rouse model, which states that a polymers of N monomers in the melt state this coefficient is

$$D = \frac{k_b T}{\xi N} \tag{2.13}$$

where ξ is the friction coefficient due to the presence of the solvent [8] .

2.2.1 Statistic of a single Ring

First of all we want to find a reference value for the radius of gyration of a polymer with a fixed length. Let us refer at this value as R_0, which is the radius of gyration of the ring at infinite diluition, computed without the interference of other rings and external factors, over a period of time long enough to be sure that the system has reached thermal equilibrium [7]. For polymer rings, with excluded volume interaction, the radius of gyration scales with the polymerization degree as $R \sim N^{\nu}$, where $\nu = 0.588$ being the Flory exponent [9].In figures 2.4 we show the behaviour of the radius for polymers rings of different length.

The first thing to notice is that, after an initial transient of time τ_r, called relaxation time, the radius fluctuates around a mean value. We assume that when this happens the system has reached the equilibrium and we take the average of R_g after the initial transient. Secondly, the relaxation time shows a dependence on the number of monomers N. In particular $\tau_r = \tau_r(N)$ increases along with N. This behavior is due to the fact that we imposed a very specific initial condition, that is a circle parallel to the xy plane. As reference value we will consider the time average, $\bar{R_0}$, of the radius after it stops decreasing and start to fluctuate. For large values of N, the relaxation time, similarly to the radius of gyration, scales as $\tau \sim N^{2\nu+1}$, accordingly to the Rouse Model, which implies that the diffusion coefficient scales as $D \sim 1/N$, as shown in equation 2.12 . We have already shown that the diffusion coefficient is proportional to the MSD, so we get

$$\Delta^2 = 2d\tau D = R_g^2 \Longrightarrow 2d\tau \frac{1}{N} \sim N^{2\nu} \Longrightarrow \tau \sim N^{2\nu+1}. \tag{2.14}$$

In table 2.2 we sumumarise the average radius of gyration for different values of N.
First of all we want to find out if $\tau_r = \tau_r(N)$ follows a power law

$$\tau_r = AN^{\alpha}$$

However we need to be careful, because we have studied polymers with number of monomers that ranges from 25 to 450. This means we can't satisfy the condition of large values of N for every ring. In order to avoid this problem, we will perform two fits. The first one considers only polymers with 150,250,300 and 450 monomers. In the second one we add a connection to scaling term as follows:

$$\tau_r = BN^{\beta}\left(1 + \frac{C}{N}\right) \tag{2.15}$$

As shown in figure 2.5, we were able to describe with good precision the how the relaxation time depends on N, both for longer and shorter rings. In particular for longer rings, illustrated in panels (b) and (c), we where able to compute a Flory exponent really close to the theoretical value $\nu = 0.588$. In fact we found

$$\alpha = 2.15 \pm 0.11 \longrightarrow \nu = 0.575 \pm 0.06$$

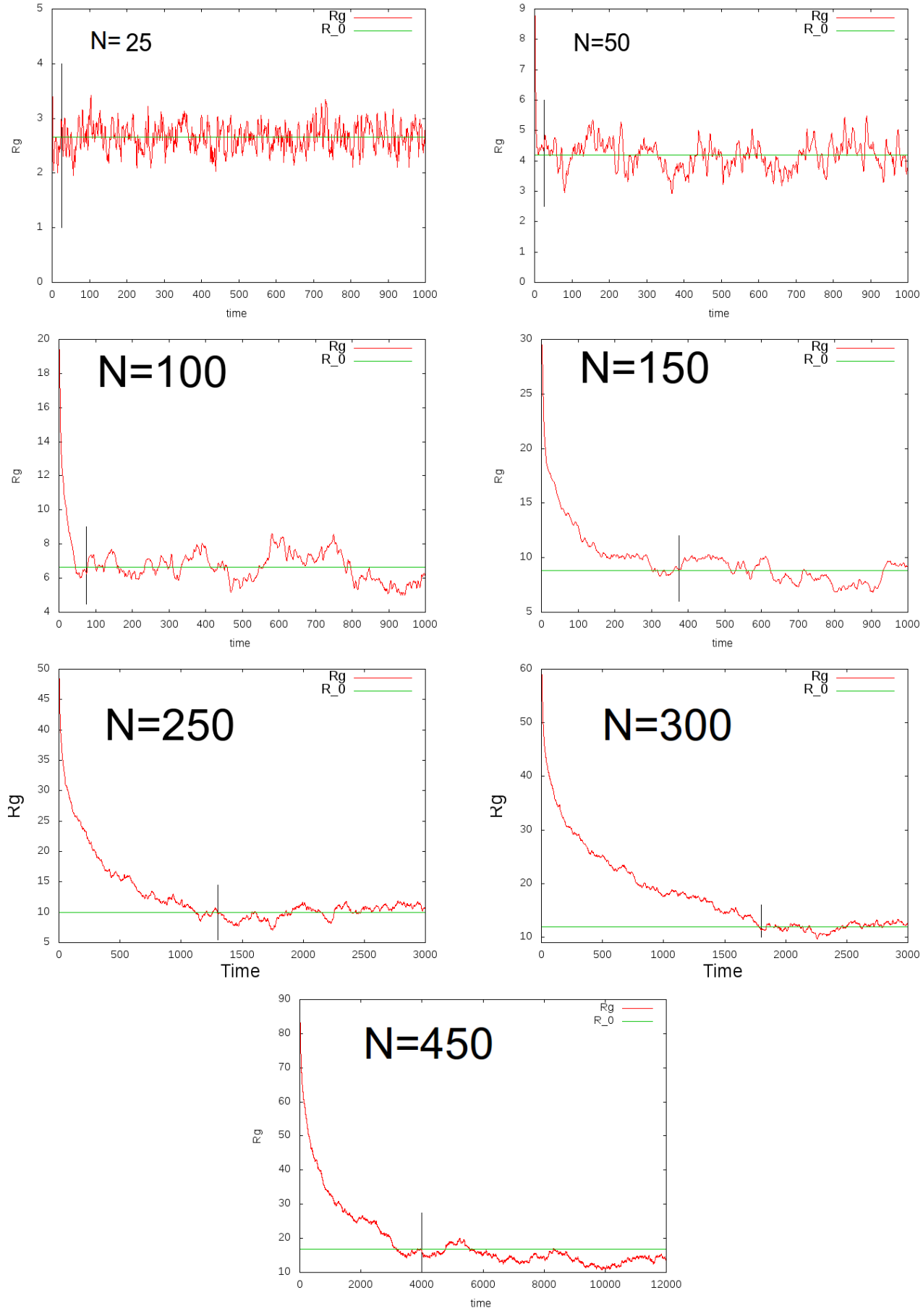

Figure 2.4: Radius of gyration as a function of time for a single ring in space, computed for rings of five different lengths. These pictures show how the relaxation time τ ,plotted as the black vertical line, is heavely influenced by the length of the ring. Moreover it is shown how for the 300-monomer and 450-monomer rings was necessary to run a simulation three and four times longer than the others to observe an equilibrium state. In table 2.2 are shown the numerical results. This are the results of a mean over five different runs.

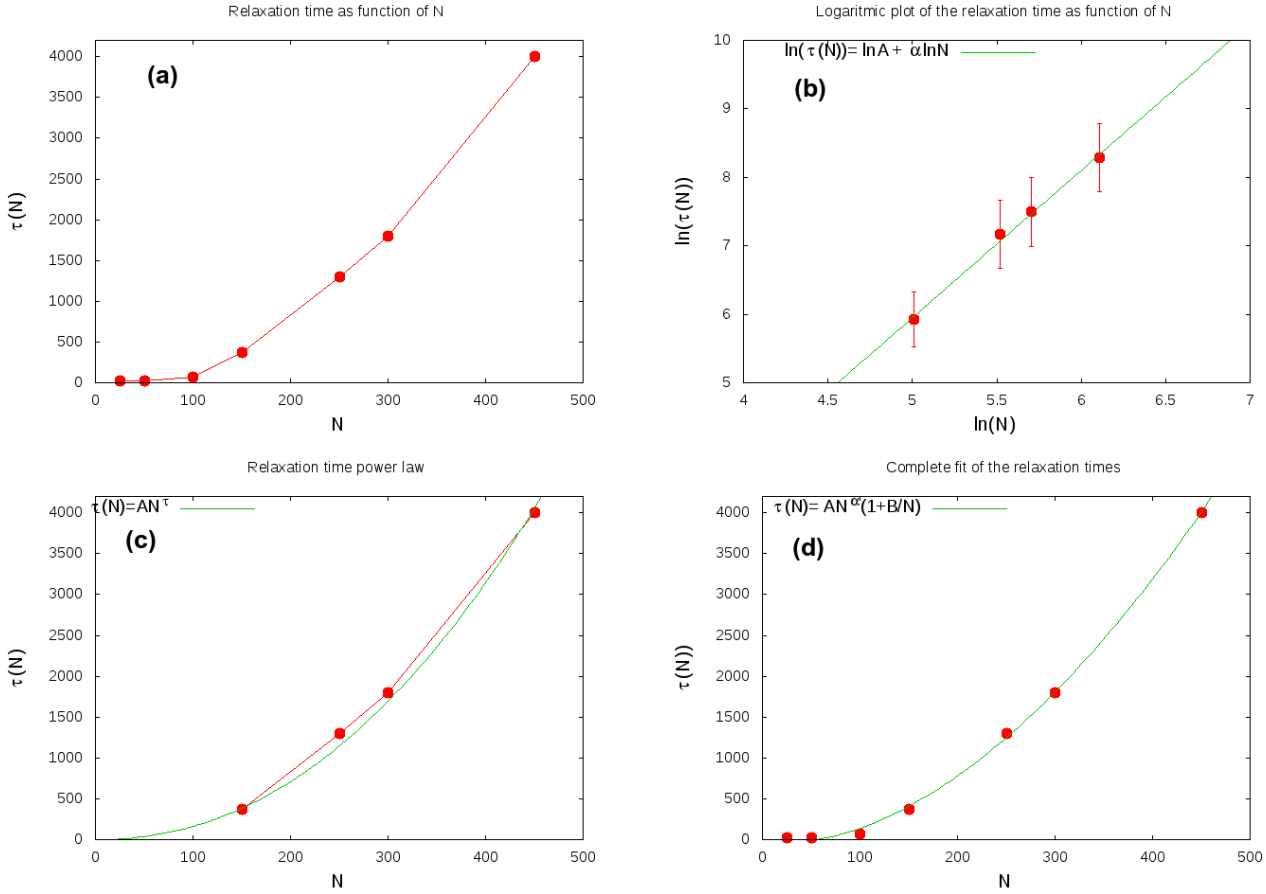

Figure 2.5: Panel (a) shows the behaviour of τ_r as function of N. Panel (b) is a logaritmic plot of the first one, where we consider only the last four points, referring to the rings with 150,250,300 and 450 monomers. We performed a linear regreassion in order to compute the parameters A and α, which lead to the results $A = 0.008 \pm 0.005$ and $\alpha = 2.15 \pm 0.11$. The third picture compares $\tau_r(N)$ with the power law AN^{α} for the four points mentioned before. Panel (d) shows the fit of all the points with the function $\tau_r = BN^{\beta}\left(1 + \frac{C}{N}\right)$, which gave the results $B = 0.1 \pm 0.2$, $\beta = 1.78 \pm 0.11$ and $C = -56 \pm 16$.

For shorter rings, as mentioned before, is impossible to estimate this exponent, however we found a connection to scaling term which allowed us to fit with precision, as shown in panel (d), the points of panel (a).

Another way to verify the scaling laws of the radius of gyration and the relaxation time is to try to collapse the curves in figure 2.4 into a single one. This can be done by redifining the axis as follows :

$$R_g \longrightarrow R_g/N^{\nu} \qquad time \longrightarrow time/t^{2\nu+1} \tag{2.16}$$

The fact that the rescaled mean values of the radius of gyration are almost the same for every ring, as you can see from table 2.3, is a confirmation that the scaling law $R \sim N^{\nu}$ is correct. The rescaled plots are shown in figure 2.6.

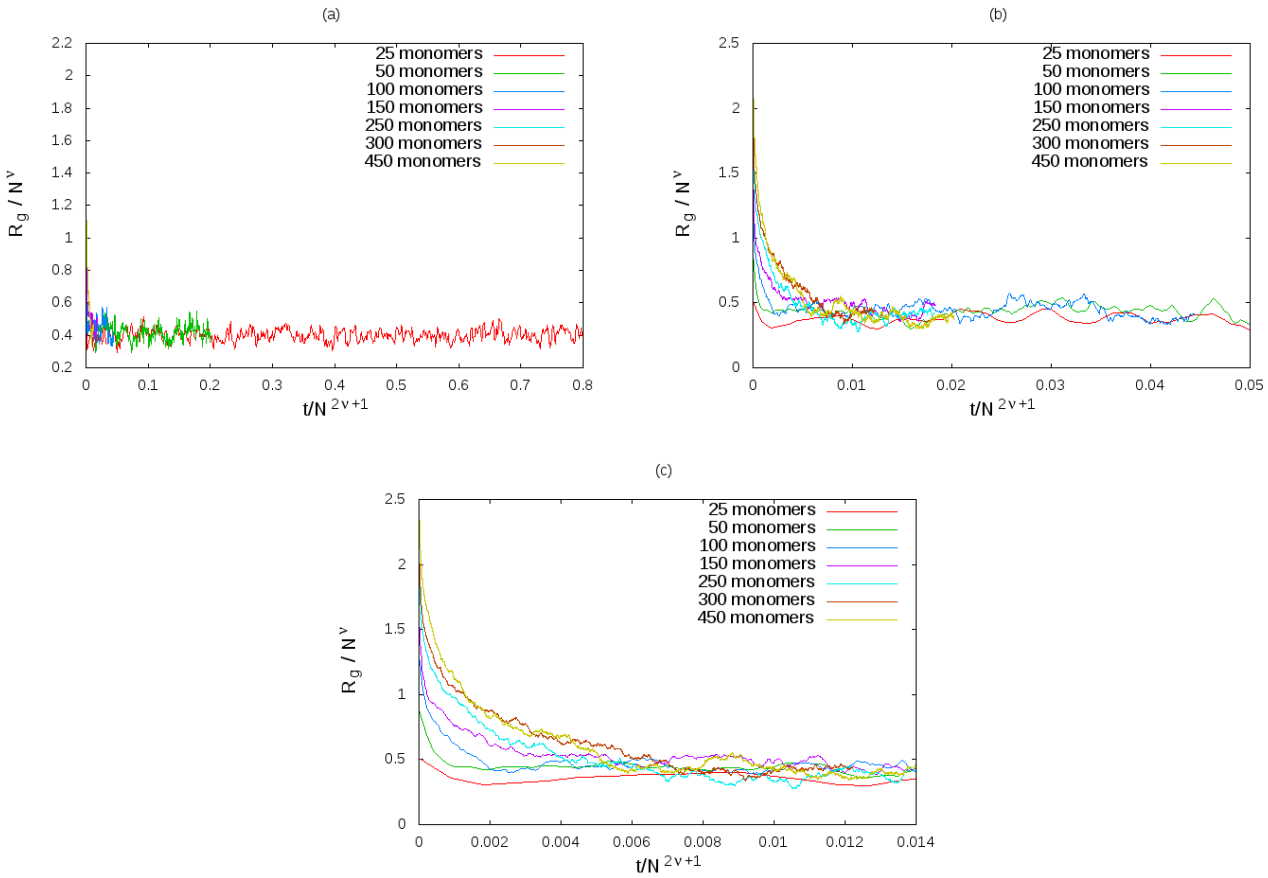

Figure 2.6: Here we show the rescaled plots of figures 2.4. Figures (b) and (c) are enlargments of the initial part of the plot in figure (a). As we can see, the curves collapse after $t/t^{2\nu+1} \sim 0.01$, while, on the other hand, at first they are distant from each other. This is probably beacuse we are working with not long enough polymers. In this case we used the theoretical Flory exponent $\nu = 0.588$.

From the plots shown in figure 2.6, we deduce that the relation $\tau \sim N^{2\nu+1}$ does not hold for our polymers, that are too short, even if for the two longest polymer the curves are almost identical. What we can try is to find a similar relation using the relaxation times τ_r listed in table 2.2, which means redfining the x-axis as follows :

$$time \longleftrightarrow time/\tau_r \tag{2.17}$$

The results of this operation are shown in figure 2.7. In this case we can seee from the plot that the curves for rings longer than 100 monomers start to get closer: the curve relative to the 100-monomere ring overlies the one related to the 150-monomere; the same thing happens for the 300-monomere and 450-monomere rings. This means that, even though the Flory relation does not hold, it should be possible to derive a similar power law which can collapse the curves into a single one.

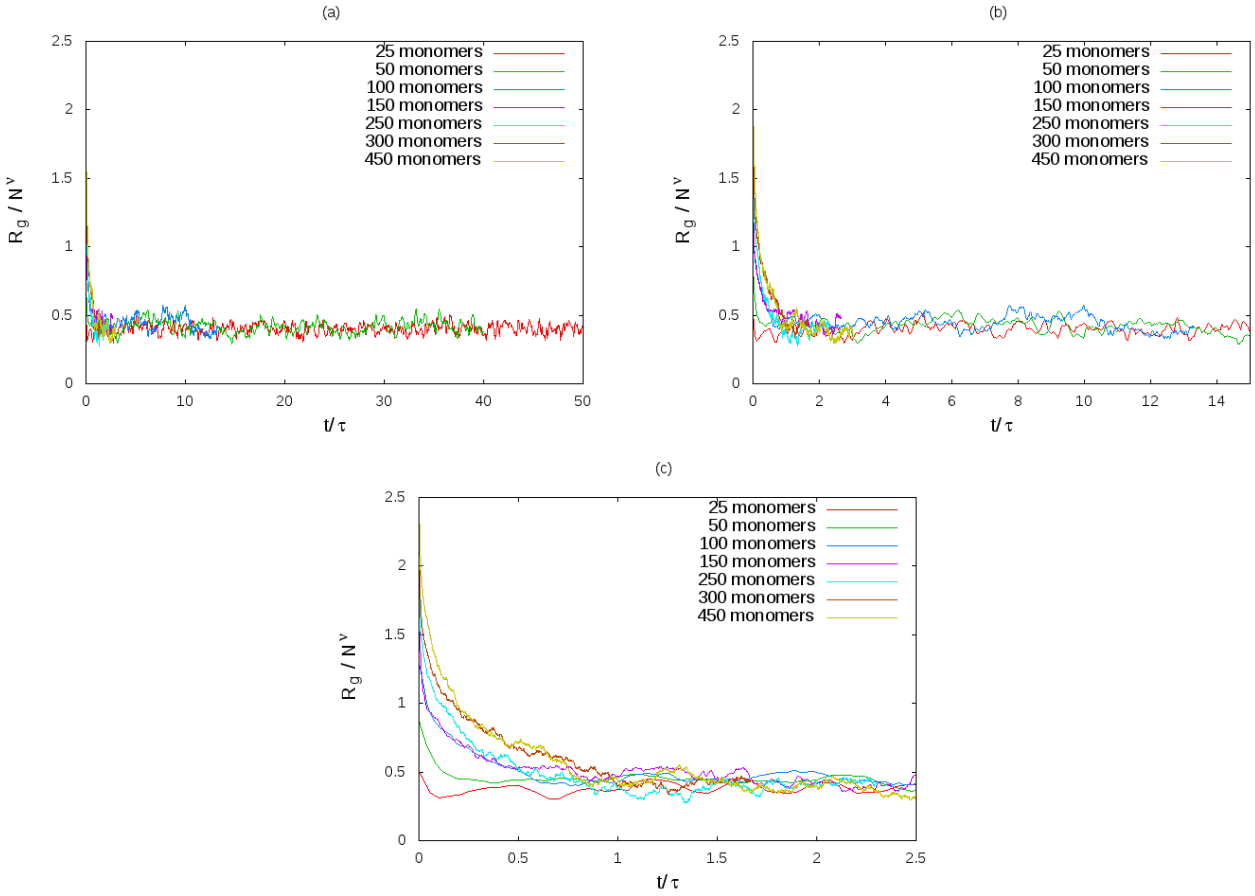

Figure 2.7: Here we show the rescaled plots of figures 2.4 using τ_r. Figures (b) and (c) are enlargments of the initial part of the plot in figure (a). As we can see, the curves collapse after $t/\tau_r = 1$, which is when the radius of gyration reaches the value $\bar{R}_0$.

N	$\bar{R}_0$	τ_r
25	2.66 ± 0.01	20
50	4.20 ± 0.02	25
100	6.64 ± 0.03	75
150	8.83 ± 0.04	375
250	9.99 ± 0.03	1300
300	11.94 ± 0.03	1800
450	14.51 ± 0.03	4000

Table 2.2: In this table are shown the time average values of $\bar{R}_0$ from figure2.4

N	$\bar{R}_0$	$\bar{R}_0/N^\nu$
25	2.66 ± 0.01	0.40 ± 0.01
50	4.20 ± 0.02	0.42 ± 0.01
100	6.64 ± 0.03	0.44 ± 0.01
150	8.83 ± 0.04	0.44 ± 0.01
250	9.99 ± 0.03	0.39 ± 0.01
300	11.94 ± 0.03	0.42 ± 0.01
450	14.51 ± 0.03	0.40 ± 0.01

Table 2.3: In this table are shown the rescaled time average values of $\bar{R}_0$. The obatained data seem to verify that the law $R_g \sim N^\nu$ applies at least for the mean values $\bar{R}_0$

Chapter 3

Effect of confinement on a single Ring

As pointed out in the introduction, polymers are heavely influenced by volume confinement. We firstly focus our attention on system composed of a single isolated ring, inside a shrinking spherical volume, and later we will study the case of a solution of multiple rings. However, due to the great computational cost necessary to have a good statistic sample, we are unable to perform an analysis similar to the one shown in the prevoius chapter. This means, for example, that we cannot find the Flory exponent for rings under confinement or analyse the scaling behaviour. Despite this limitations, we are still able to describe important charateristics, such as the evolution of the radius of gyration and the diffusion coefficient.
We considered two different systems, one with a 150-monomer ring and one with 300-monomer ring. Then we observe their behoviur inside different shrinking volumes: we start from the same initial sphere, but then we change the final value of the sphere radius. In this way we were able to study the behaviour of the two isoleted rings in six different shrinking volumes. For each volume, and both rings, we run twenty independent simulations so that we could properly compute mean values with a good statistics.

3.0.1 Parameters of the simulations

The parameters of the simulation for this part of the study are basically the same that we used in the previous sections, with some additions. We still have FENE, cut Lennard-Jones potentials and Langevin dynamics; with the same parameters described in Chapter 2.
What we need to specify here are the different sphere radii, and the features of the sphere surface. As said before we used six different values for the radius, which are, in Lennard-Jones units: $R_s = 30, 20, 15, 10, 5, 2.5$.
We then described the sphere surface as a bounding wall which interacts with nearby particles. The energy of wall-particle interactions is described with the 9/3 potential :

$$V_{9/3} = \epsilon \left[\frac{2}{15} \left(\frac{\sigma}{r} \right)^9 - \left(\frac{\sigma}{r} \right)^3 \right] \tag{3.1}$$

where r is the distance between the surface and particles. The distance between a particle and the surface is the distance to the nearest point on the surface and the force the wall exerts on the particle is along the direction between that point and the particle, which is the direction normal to the surface at that point. This potential as a non-zero value only for $r < r_c$, where r_c is a cutoff distance at which the particle and surface no longer interact. In our specific case we have : $\sigma = 1.0$, $\epsilon = 1.0$ and $r_c = 1.122$.

R_s	Φ	R_s^{-1}	$\bar{R}_{150}$	$\bar{R}_{300}$
30	0.00069	0.033	7.87 ±0.04	12.12 ±0.02
20	0.00234	0.05	7.82 ±0.04	10.70 ±0.02
15	0.00555	0.067	7.60 ±0.08	9.26 ±0.04
10	0.01875	0.1	6.25 ±0.2	7.01 ±0.3
5	0.15000	0.2	4.07 ±0.3	4.36 ±0.5
2.5	1.20000	0.4	2.80 ±0.5	3.19 ±0.6

Table 3.1: Data obtained for both 150-monomer and 300-monomer ring inside the shrinking sphere. These results are plotted in figure (3.1).

3.0.2 Effects of confinement on the radius of gyration

In this part we describe quantitatively what happens to the radius of gyration subject to confinement. The initial condition of the simulation is a circle-shaped ring parallel to the xy which follows the dynamic introduced in subsection (2.1.3). First, in order to equilibrate the system, we perform a run with simulation time $t = 500$ where the radius of the sphere decrease from $R = 68.0$ to R_S; then, when the ring is succesfully confined inside a sphere with radius R_S, we perform a second run with simulation time $t = 5000$ from which we compute the radius of gyration. We focus our attention to the rings with $N = 150$ and $N = 300$. Notice that simulation time $t = 5000$ is bigger then τ_b for the rings taken into account, in order to let the system reach an equilibrium.

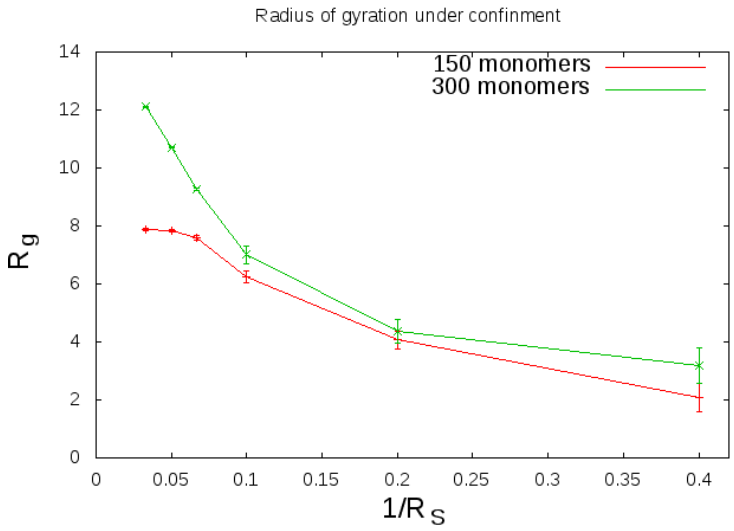

Figure 3.1: In this plot we show how the radius of gyration of a single isolated ring reacts to confinement. We can see that the two curves, red for the 150-monomer ring and green for the 300-monomer ring, start to show a similar behaviour when $1/R_S \sim 0.1$. In particular the typical dependence $R_g \sim N^\nu$ disappears for $1/R_S \leq 0.1$

In figure 3.1 we show how the radius of gyration changes after confinement, while in figure 3.1 are reported the data used for the plot.

One can see that for sufficiently strong confinemet ($\frac{1}{R_s} = 0.1$) the average size of the rings do not grow with N and start to fill the space inside the sphere. A change in the ring conformation is expected. The value $1/R_S$ where this new regime starts should depend on N as well : we expect that for greater N, the critical point $1/R_S$ should be smallers. However we are not able to verify this assumption, since we have only two curves.

3.0.3 Computation of the diffusion coefficient

We have already shown that the diffusion coefficient is linked to the Δ^2 of the ring center of mass through the relation

$$\Delta^2 = 2d\tau. \tag{3.2}$$

The data necessary for us to compute Δ^2 are obtain from the same simulation used to compute the radius of gyration. In order to evaluate the coefficient D we make use of another relation :

$$\lim_{t\to+\infty} \frac{\Delta^2}{t} = 2dD \tag{3.3}$$

In fact, using the latter relation we can estimate the time interval in which the rings properly follow a brownian dynamic. More precisely we build a plot with $\frac{\Delta^2}{t}$ on the y-axis and lnt on the x-axis; we are interested in the part of the plot that shows a curve parallel to the x-axis. This section of the plot gives us a first value of D and an interval of time Δt. Then it is possible to use the logaritmic plot of the points $(\Delta^2, 2dDt)$, with $d = 3$ inside the interval Δt to gain a more precise value of the diffusion coefficient, in fact we obtain the realation

$$ln\Delta^2 = ln(2dD) + lnt = ln(6D) + lnt \tag{3.4}$$

which allows us to estimate $ln(6D)$ by means of a linear regression

Before starting this analysis we need to figure out if it is reasonable to compute the MSD of the center of mass for every value of R_S that we chose: we expect that for small values of R_S the ring is unable to diffuse, impling that the MSD is essentially zero. In order to verify this assumption we look at the plot of Δ^2 (150-monomer ring) from a single simulation for all the six values of R_S used. This hypotesis, as shown in figure 3.2 seems to be correct, hence we focus our attention only at the cases with $R_S = 30, 20, 15, 10$. The same kind of reasoning can be applyed to the case of the 300-monomer ring, obtaining identical results.

In figures 3.3, 3.4, 3.5 and 3.6 are shown, as example, some of the plots regarding the analysis explained right before. As we can see, finding a correct intervall Δt sometimes can be very challenging; a possible way to solve this problem is to improve the statistic of our data sample, but this would imply a greater computational effort, which we cannot afford. This problem, as is it possible to see from the numerical result shown in tables 3.2 and 3.3, leads to a discrepancy between the values of the diffusion coefficient D computed in the two different ways : the mean of the points inside Δt, and the fit of the logaritmic plot.
Since the results deriving from fit are more accurate, we assume that they give us the best value of D. Notice that the value of D gets smaller as the volume decreases, meaning that the ring loses mobility, and it is more difficul for it to diffuse at lower R_S.

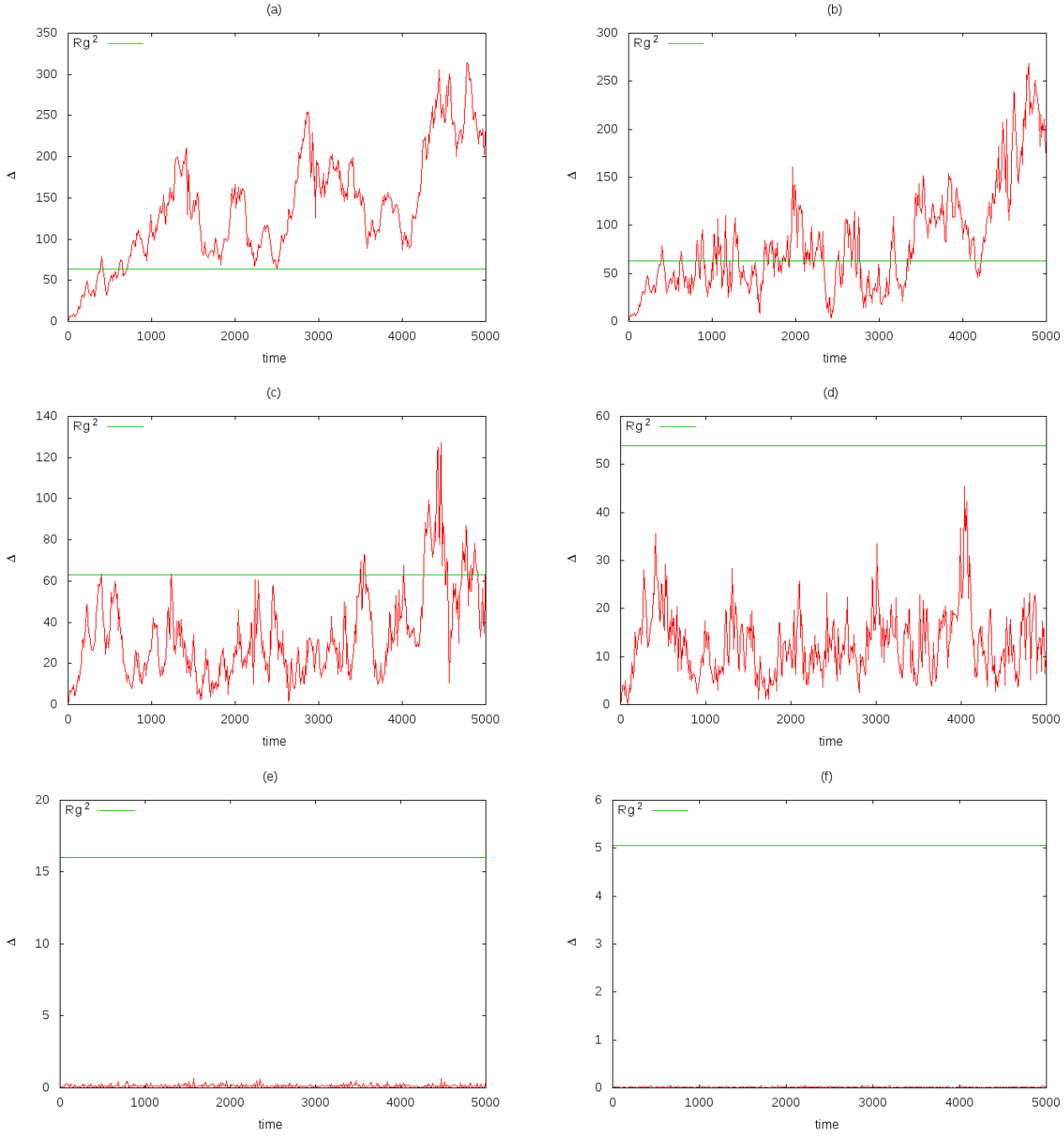

Figure 3.2: In This figures is plotted the MSD of the center of mass for the 150-monomer ring with six different values of R_S, in red, and R_g^2, in green. Figure (e) and (f) show that the MSD for $R_S = 5$ and $R_S = 2.5$ is basically zero, in fact we only see small fluctuations.

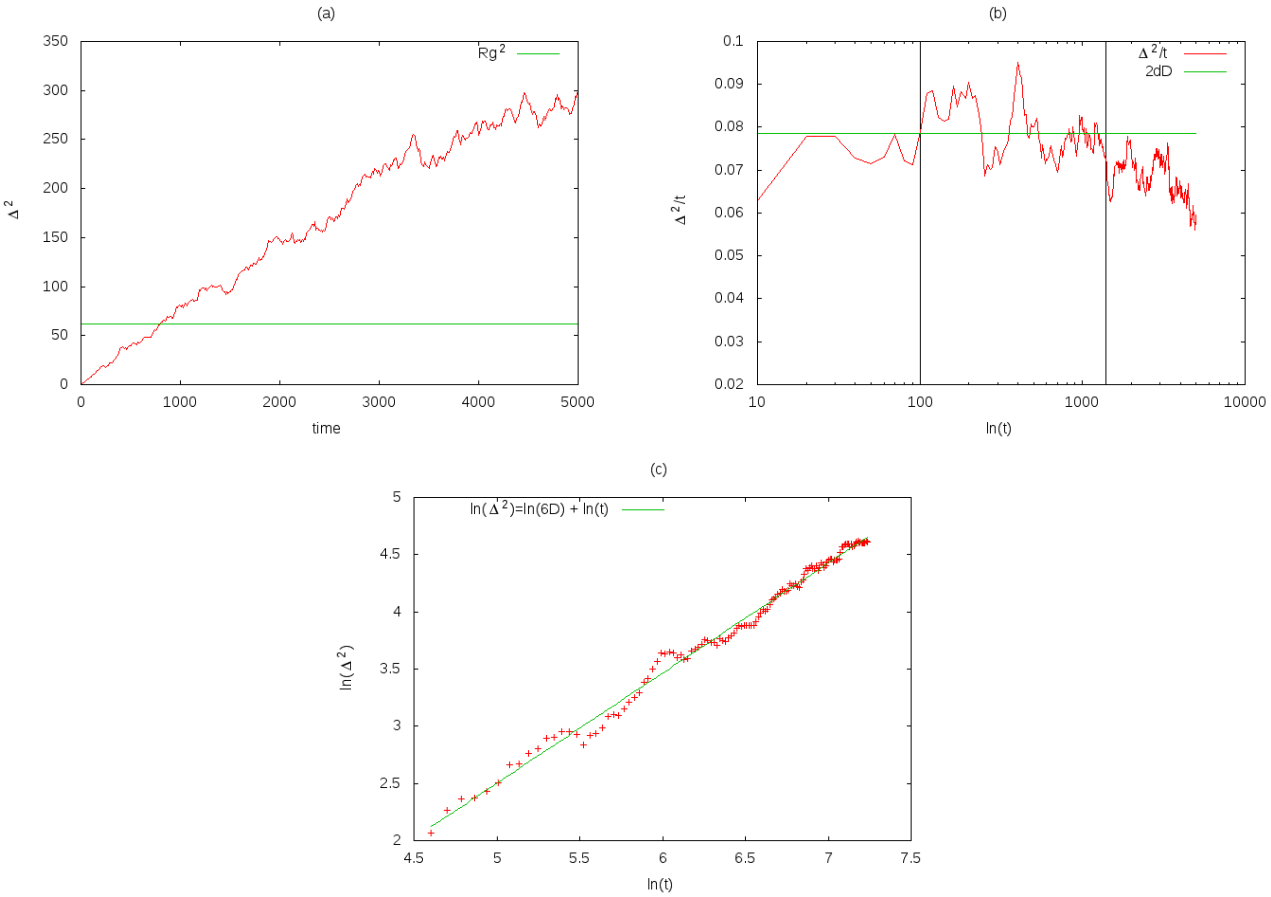

Figure 3.3: Here we show the MSD of the center of mass, its logaritmic plot, and the plot of the points $(\Delta^2/t, t)$ for a 150-monomer ring and $R_s = 30$. Figure (a) is relative to Δ^2; figure (b) shows the points $(\Delta^2/t, t)$, where it is possible to see the interval Δt between the black vertical lines and a first guess of $6D$ (green line); figure (c) shows the logaritmic plot of figure (a) inside the intervall Δt.

R_S	$\Delta t \cdot 10^{-2}$	$D_{\Delta t} \cdot 10^{-2}\sigma(\frac{\epsilon}{m})^{1/2}$	$D_{fit} \cdot 10^{-2}\sigma(\frac{\epsilon}{m})^{1/2}111$
30	[100,1400]	1.31 $\pm$0.2	1.65 $\pm$0.12
20	[100,1000]	1.29 $\pm$0.2	1.75 $\pm$0.25
15	[100,400]	0.99 $\pm$0.3	0.68 $\pm$0.44
10	[10,100]	0.98 $\pm$0.4	0.49 $\pm$0.27

Table 3.2: Data obtained for 150-monomer ring; we can notice that for the first two R_S the values of the diffusion coefficients are similar, but for the last two values of R_S they are drastically different.

R_S	Δt	$D_{\Delta t} \cdot 10^{-3}\sigma(\frac{\epsilon}{m})^{1/2}$	$D_{fit} \cdot 10^{-2}\sigma(\frac{\epsilon}{m})^{1/2}111$
30	[50,300]	7.16 $\pm$0.22	1.81 $\pm$0.12
20	[20,200]	6.01 $\pm$0.25	1.12 $\pm$0.25
15	[30,200]	6.41 $\pm$0.71	0.56 $\pm$0.04
10	[40,130]	8.16 $\pm$0.8	0.49 $\pm$0.09

Table 3.3: Data obtained for 300-monomer ring.

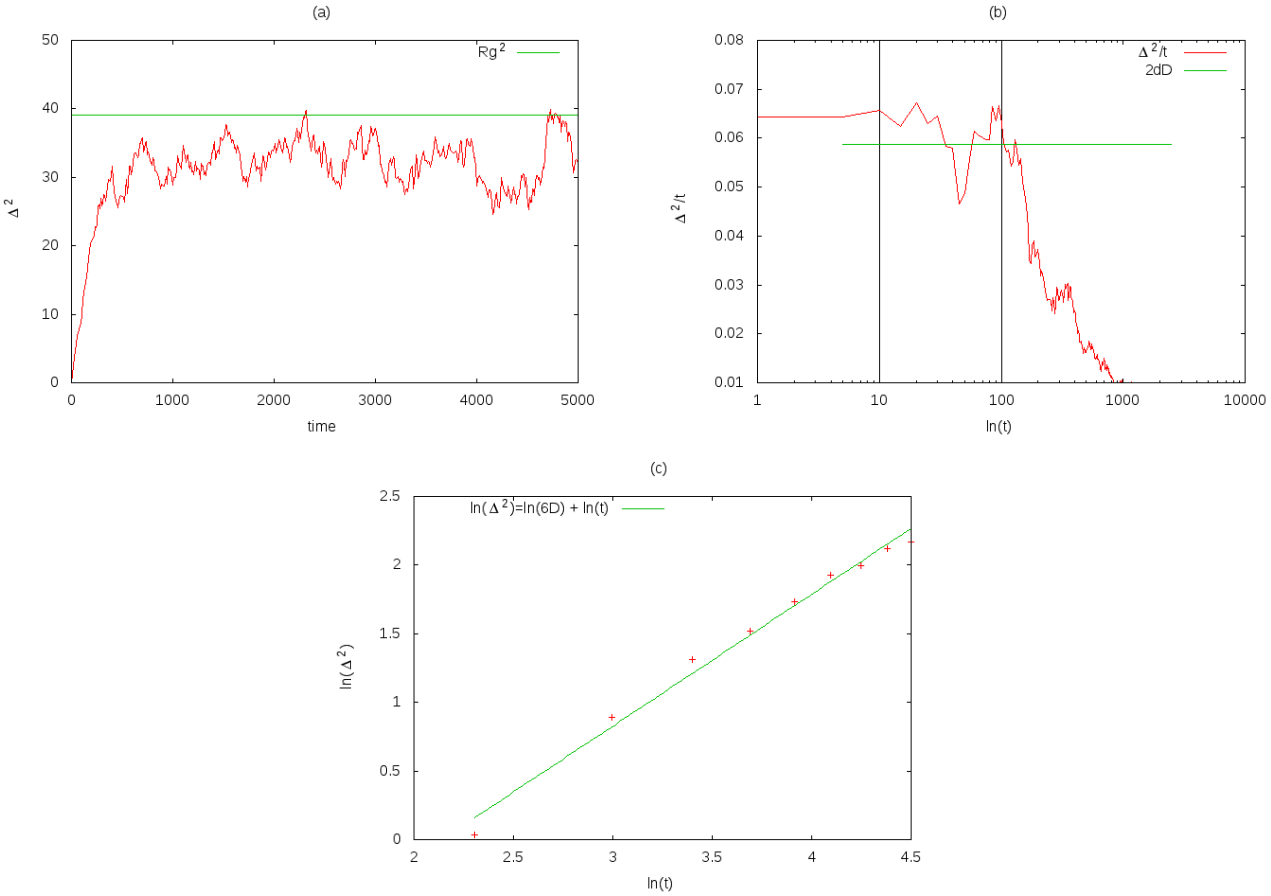

Figure 3.4: Here we show the same plots of figure 3.3, but with R_S=10. Notice that it is much more difficult to estimate with good precision Δt, which is also significantly smaller. This happens because the system reaches a saturation point faster than the case with $R_S = 30$, as can be seen from figure (a), where the curve rapidly increases at the beginning and then starts to oscillate. Moreover, the shortness of the intervall Δt, reflects negatively on the precison of the logaritmic fit since we have less points at our disposal.

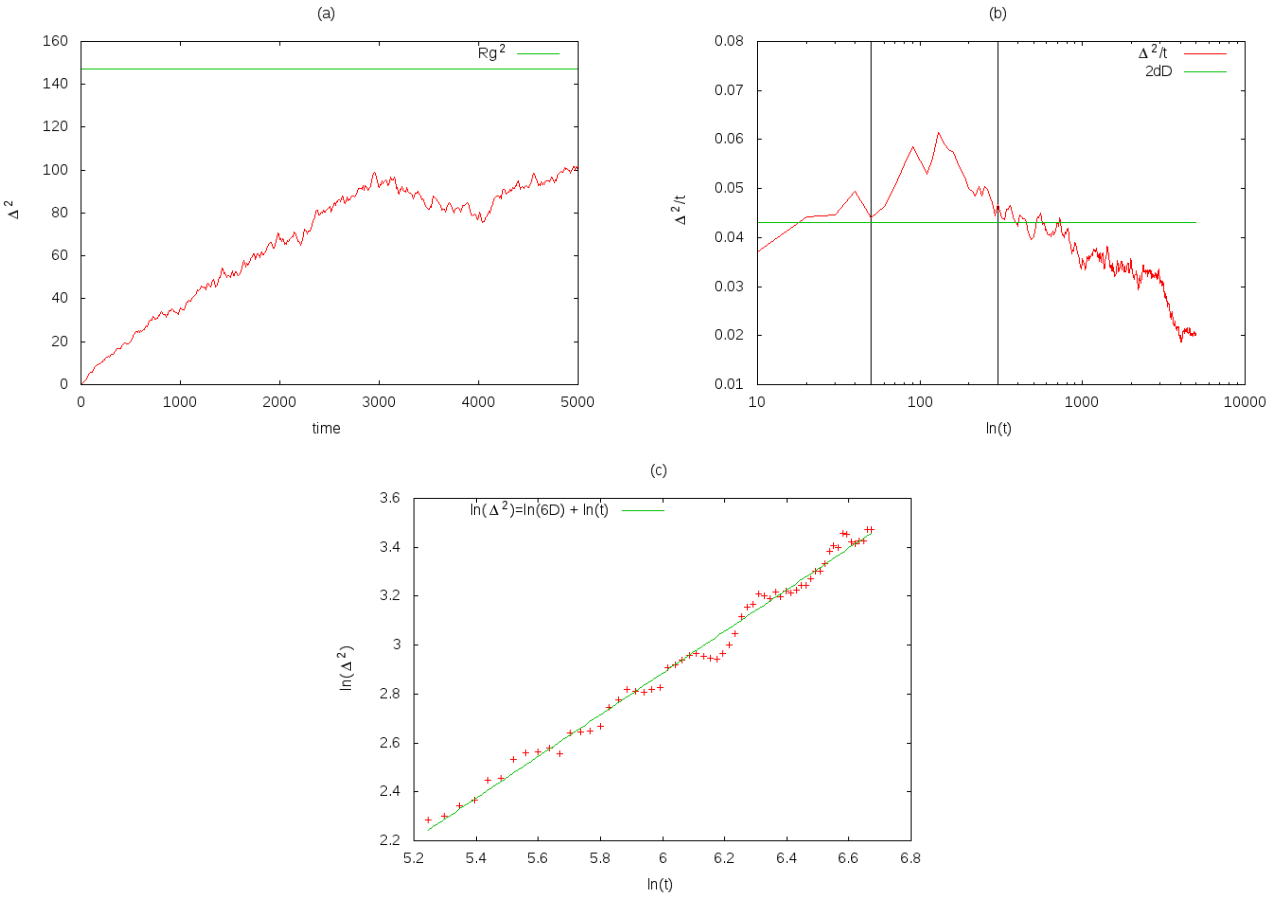

Figure 3.5: This is the same of figure 3.3 but for a 300-monomer ring and $R_S = 30$

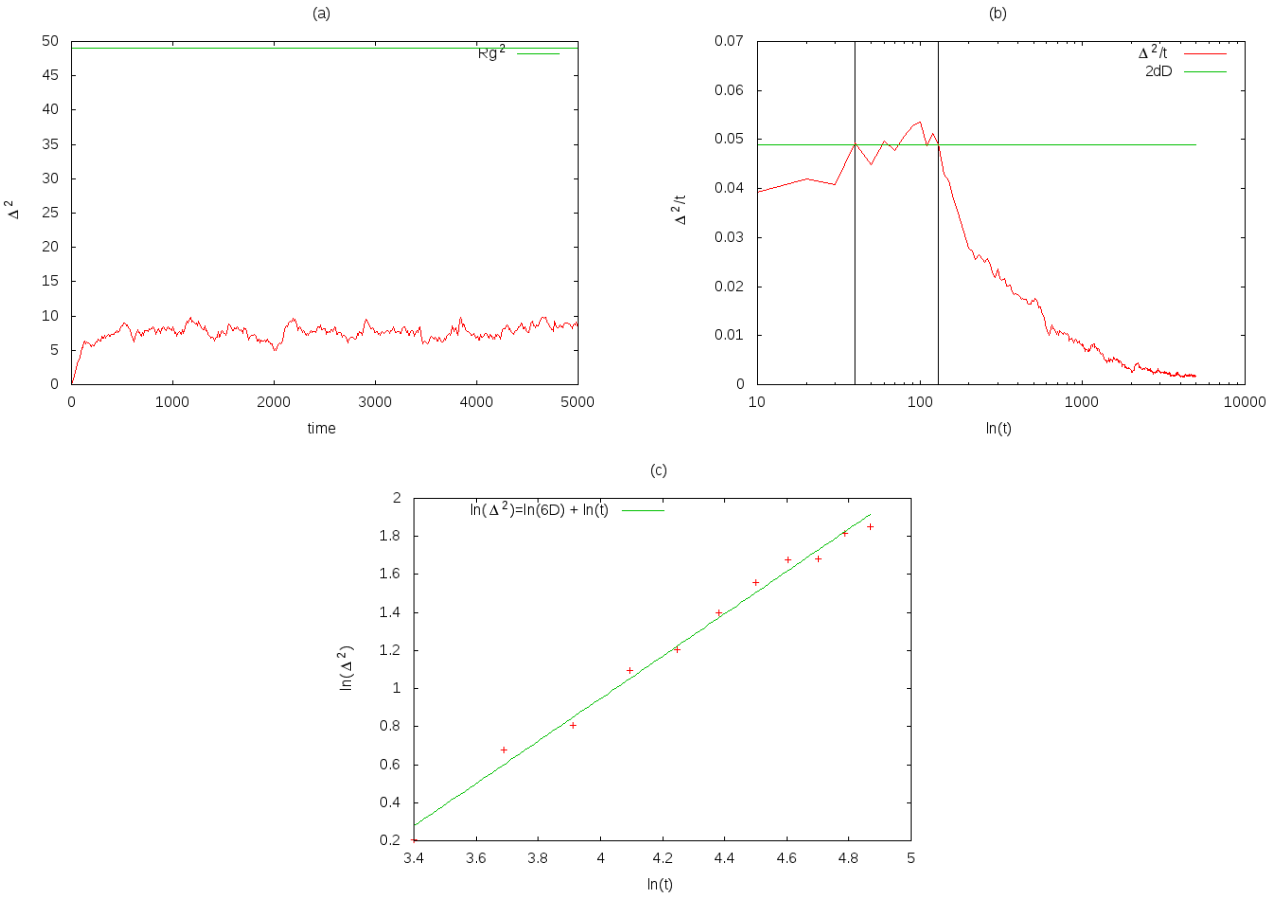

Figure 3.6: This is the same of figure 3.3 but for a 300-monomer ring and $R_S = 10$

Chapter 4

Solutions of several Rings

We now consider more the one ring in solution. We consider, as we have already done before, two cases: one in which the rings are in a periodic box and the other in which they are confined within a sphere. As seen before, it is possibile to characterize the system by the quantity Φ. Initially we are interested in comparing the two geometries with the condition $\Phi_{box} = \Phi_{sphere}$. Since the total number of monomers is fixed, this condition implies $V_{box} = V_{sphere}$. The procedure is the same used in the previous section: we compute the time average of the radius of gyration after discarding all the values prior to τ. In tables **??** and **??** we show the results for $N = 150$ and $N = 300$ with different number of rings.

Table 4.1: Results for $\Phi = 78 \cdot 10^{-6}$ ($N = 150$) inside the box

N_R	$\bar{R}_g(N_R = 1)$
1	10.42 ± 0.03

N_R	$\bar{R}_g(N_R = 3)$
	4.26 ± 0.02
3	4.17 ± 0.02
	4.39 ± 0.04

N_R	$\bar{R}_g(N_R = 6)$
	2.647 ± 0.004
	2.627 ± 0.004
6	2.595 ± 0.004
	2.639 ± 0.004
	2.644 ± 0.004
	2.584 ± 0.004

Table 4.2: Results for $\Phi = 156 \cdot 10^{-6}$ ($N = 300$) inside the box

N_R	$\bar{R}_g(N_R = 1)$
1	11.84 ± 0.02

N_R	$\bar{R}_g(N_R = 6)$
	6.42 ± 0.02
3	6.72 ± 0.01
	6.03 ± 0.01

N_R	$\bar{R}_g(N_R = 6)$
	4.117 ± 0.006
	4.016 ± 0.006
6	4.177 ± 0.006
	4.345 ± 0.006
	4.133 ± 0.006
	3.975 ± 0.006

The results show that, in these cases, there are not particular differences between R_0 and $Rg(N_R)$. This is due to the fact that $\Phi = 156 \cdot 10^{-6}$ and $\Phi = 78 \cdot 10^{-6}$, meaning an extremely diluted solution where the rings do not interact one to another. In order to see a more relevant

Table 4.3: Results for $\Phi = 78 \cdot 10^{-6}$ ($N = 150$) inside the sphere

N_R	$\bar{R}_g(N_R = 1)$
1	8.16 ± 0.05

N_R	$\bar{R}_g(N_R = 3)$
	4.06 ± 0.02
3	4.02 ± 0.02
	4.08 ± 0.02

N_R	$\bar{R}_g(N_R = 6)$
	2.45 ± 0.01
	2.42 ± 0.01
6	2.43 ± 0.01
	2.43 ± 0.01
	2.42 ± 0.01
	2.44 ± 0.01

Table 4.4: Results for $\Phi = 156 \cdot 10^{-6}$ ($N = 300$) inside the sphere

N_R	$\bar{R}_g(N_R = 1)$
1	13.15 ± 0.14

N_R	$\bar{R}_g(N_R = 3)$
	6.33 ± 0.03
3	6.34 ± 0.03
	6.22 ± 0.04

N_R	$\bar{R}_g(N_R = 6)$
	4.09 ± 0.01
	4.12 ± 0.01
6	4.06 ± 0.01
	4.03 ± 0.01
	4.03 ± 0.01
	4.10 ± 0.01

interaction between the polymers we consider simulation where the system's volume is gradually decreased. In figure 4.1 we show the results for a solution of three rings.

4.0.1 Depencence of $\bar{R}_g(N_R)$ on Φ

We now look at the behaviour of the radius of gyration of one ring as the volume of the system decreases, to observe the effects of confinement and concentration on the topology of the rings. In the previous sections we had a cubic box with $L = 100$ and a sphere with $R = 62.5$. The computation is divided in two steps: first we run a simulation inserting the polymers in a periodic box with $L = 100$, as before, which decreases in time until it reaches a given value $L = L_b$,in order to equilibrate the system at $t >> \tau$; in figure 4.2 are shown the initial and equilibrion conditions. Afterwards we run a longer simulation to see how the radius of gyration changes inside a smaller volume.After we procede in the same way for a sphere with hard walls,by imposing $\Phi_{sphere} = \Phi_{box}$. We chose six different values of L_b and R_s. In figure 4.3 and 4.4 are shown the results.
What we can see from the figures, in both cases, is that for longer rings the radius of gyration has a more steep change respect to the shorter ones. Moreover we notice that there is a drastic change in the value of the radius of gyration when the system reaches a situation where $R_g \simeq L_b$.

In figure 4.5 and 4.6 we show the results obtained from the same process done with the sphere. The behavior of the radius of gyration is similar to the one noticed in the previous case; however for the lowest values of Φ notice that the values of R_g are significantly higher than the

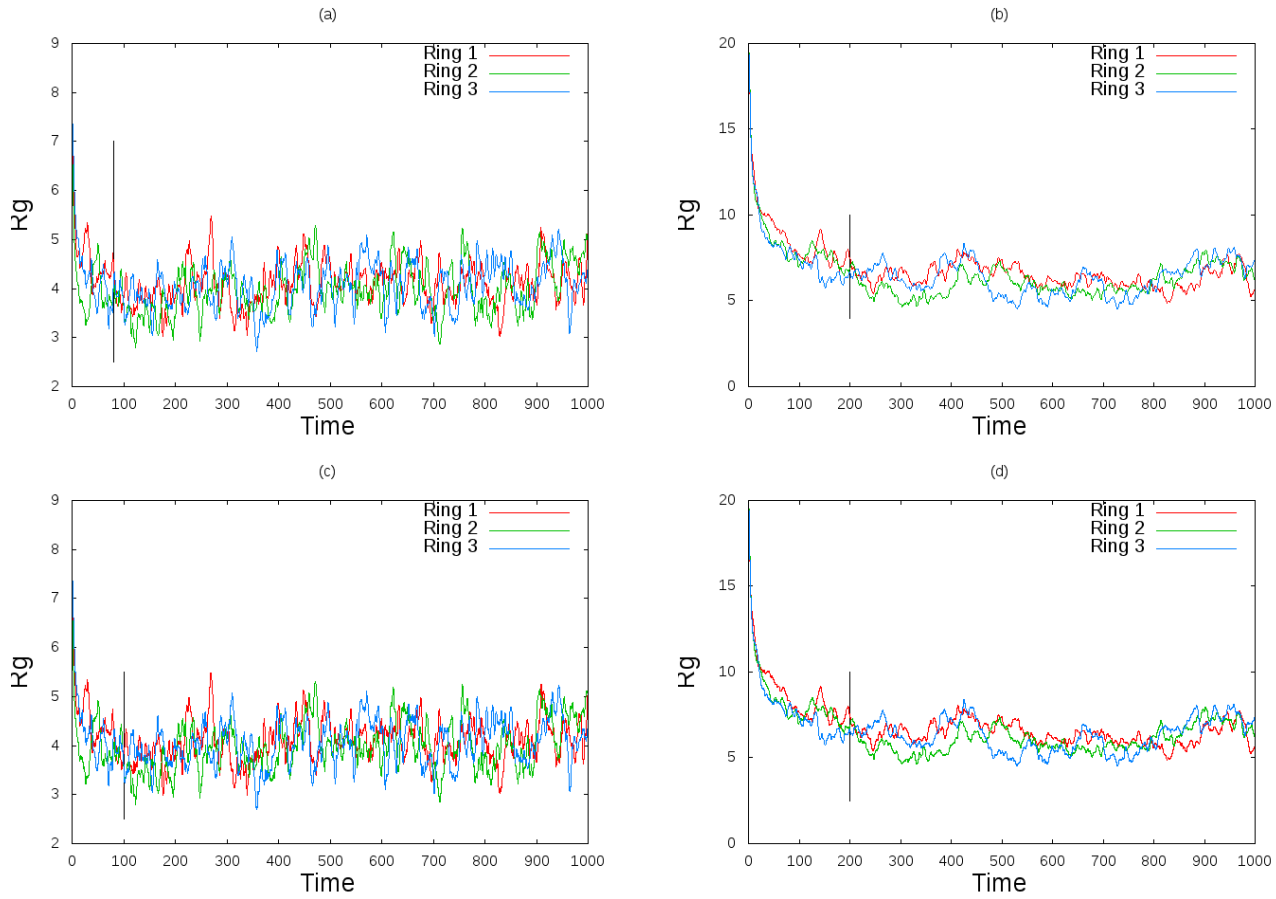

Figure 4.1: Radius of gyration as a function of time for a solution of three rings. In figure **(a)** and **(b)** are shown the results for the periodic box, respectively with 150 and 300 total number of monomers. Figure **(c)** and **(d)** show the same for the sphere. We decided to bring only this example because it is the only one where we can find a difference from what we studied in the previous section: the relaxation time τ is bigger; more precisely we have $\tau^{box}_{150} = 80$, $\tau^{box}_{300} = 200$,$\tau^{sp}_{150} = 100$, $\tau^{sp}_{300} = 200$.

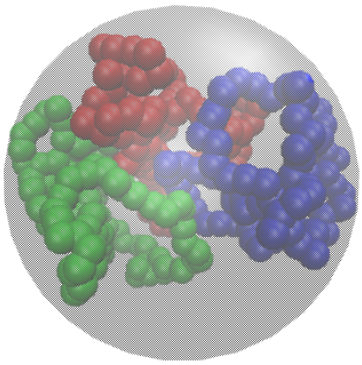

Figure 4.2: Example of a configuration with three rings inside a sphere with N=300 and $R_S = 10$

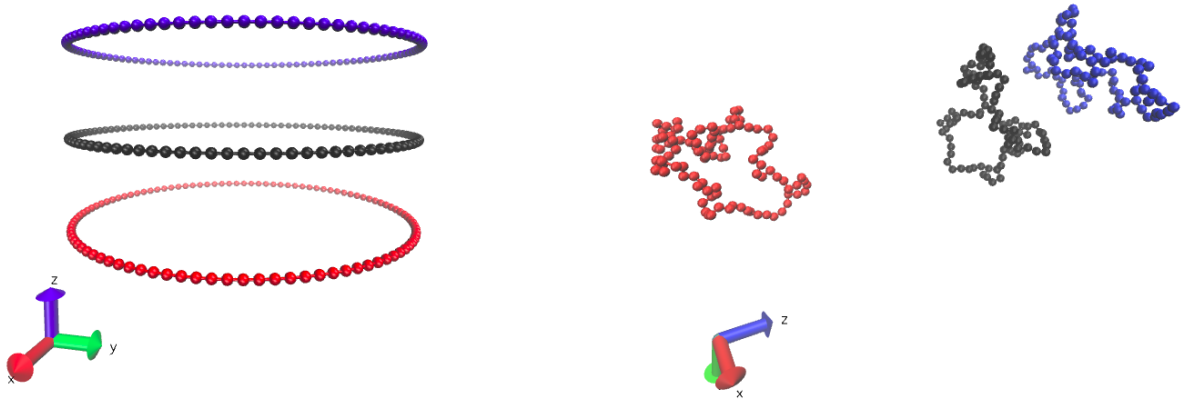

Figure 4.3: On the left is shown an exemple of a systems initial condition, where three rings are circle shaped and aligned along the z- axis. On the right is it possible to see the same system at the equilibrium condition, after the shrinking of the volume is complete

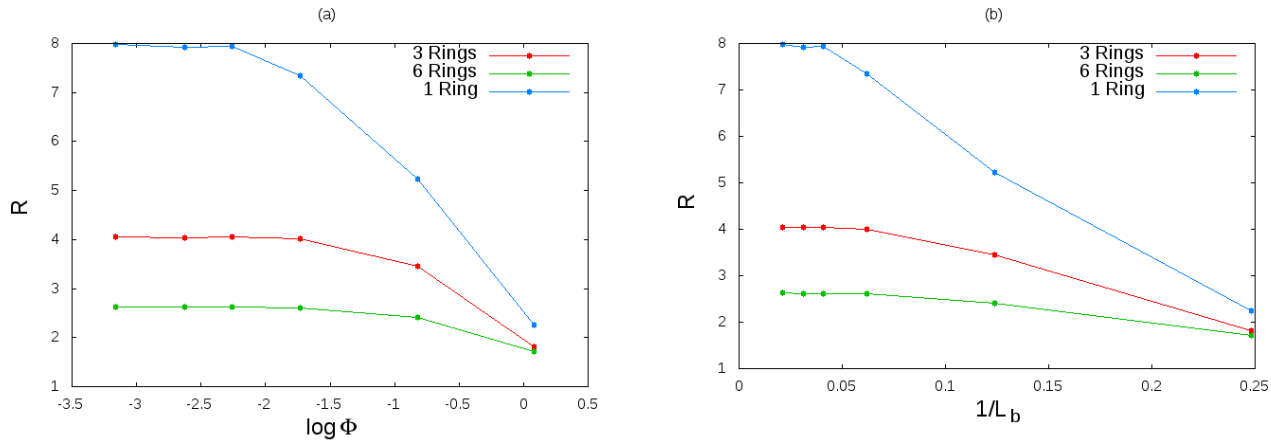

Figure 4.4: In these figures are shown the results obtained for 150-monomers rings inside the periodic box. In figure **(a)** is shown the relation between ϕ and $\bar{R}_g$, while in figure **(b)** is shown the relation between L_b and $\bar{R}_g$.

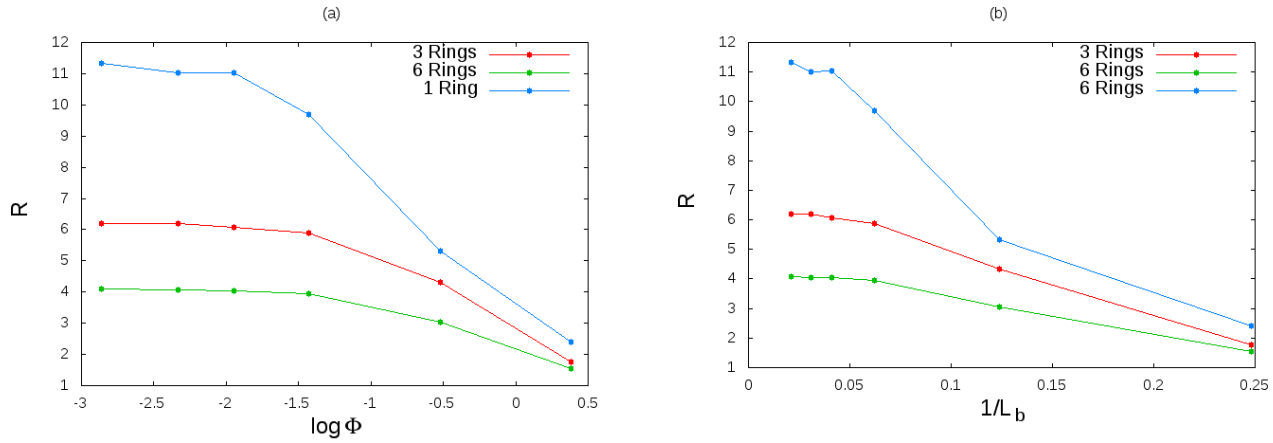

Figure 4.5: In these figures are shown the results obtained for 300-monomers rings inside the periodic box. In figure **(a)** is shown the relation between ϕ and $\bar{R}_g$, while in figure **(b)** is shown the relation between L_b and $\bar{R}_g$.

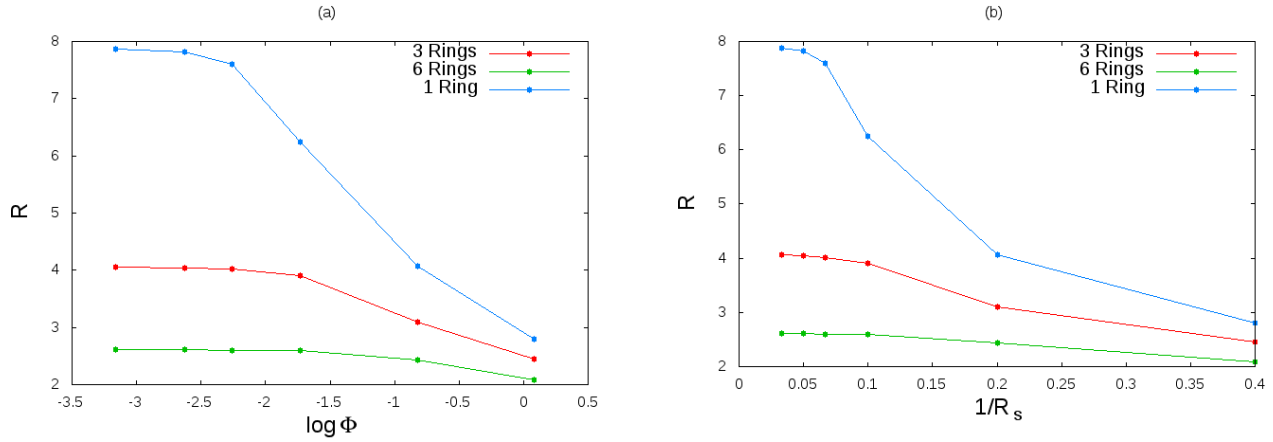

Figure 4.6: In these figures are shown the results obtained for 150-monomers rings inside the sphere. In figure **(a)** is shown the relation between ϕ and $\bar{R}_g$, while in figure **(b)** is shown the relation between R_s and $\bar{R}_g$.

R_s	Φ	R_s^{-1}	$\bar{R}_1$	$\bar{R}_3$	$\bar{R}_6$
30	0.00069	0.033	7.87 $\pm$0.04	4.06 $\pm$0.02	2.62 $\pm$0.01
20	0.00234	0.05	7.82 $\pm$0.04	4.04 $\pm$0.02	2.62 $\pm$0.01
15	0.00555	0.067	7.60 $\pm$0.03	4.02 $\pm$0.02	2.60 $\pm$0.01
10	0.01875	0.1	6.25 $\pm$0.02	3.91 $\pm$0.02	2.59 $\pm$0.01
5	0.15000	0.2	4.07 $\pm$0.01	3.10 $\pm$0.02	2.43 $\pm$0.01
2.5	1.20000	0.4	2.80 $\pm$0.01	2.45 $\pm$0.01	2.08 $\pm$0.01

Table 4.5: Data obtained for 150 monomers inside the sphere

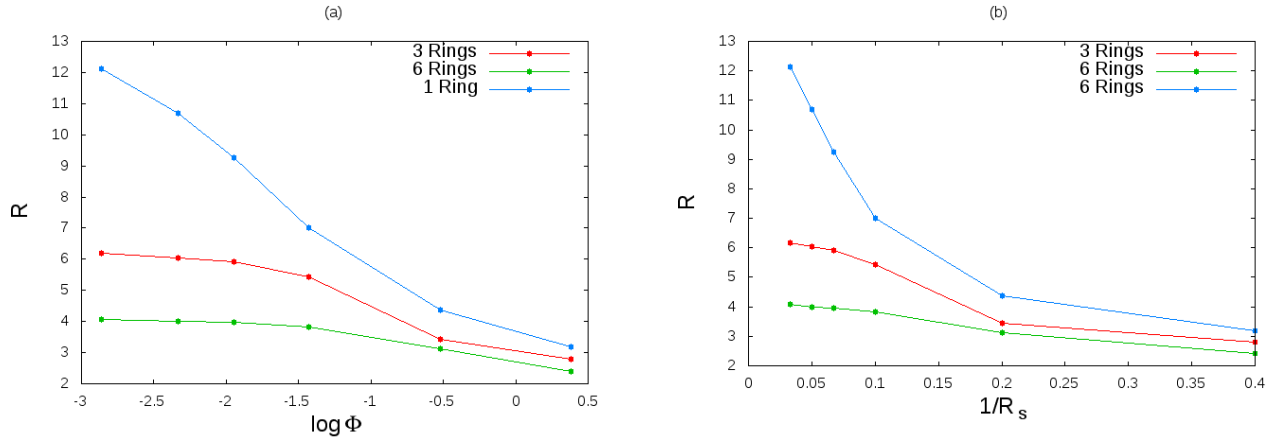

Figure 4.7: In these figures are shown the results obtained for 300-monomers rings inside the sphere. In figure **(a)** is shown the relation between ϕ and $\bar{R}_g$, while in figure **(b)** is shown the relation between R_s and $\bar{R}_g$.

R_s	Φ	R_s^{-1}	$\bar{R}_1$	$\bar{R}_3$	$\bar{R}_6$
30	0.00069	0.033	12.12 $\pm$0.06	6.18 $\pm$0.04	4.07$\pm$0.01
20	0.00234	0.05	10.70 $\pm$0.03	6.05 $\pm$0.03	4.00$\pm$0.01
15	0.00555	0.067	9.26 $\pm$0.03	5.92 $\pm$0.03	3.96$\pm$0.01
10	0.01875	0.1	7.01 $\pm$0.01	5.42 $\pm$0.02	3.82$\pm$0.01
5	0.15000	0.2	4.36 $\pm$0.01	3.44 $\pm$0.03	3.12 $\pm$0.01
2.5	1.20000	0.4	3.18 $\pm$0.01	2.79 $\pm$0.01	2.41$\pm$0.01

Table 4.6: Data obtained for 300 monomers inside the sphere

L_b	Φ	L_b^{-1}	$\bar{R}_1$	$\bar{R}_3$	$\bar{R}_6$
48.36	0.00069	0.021	7.97 ±0.04	4.05 ±0.02	2.63 ±0.01
32.24	0.00234	0.03 1	7.92 ±0.04	4.04 ±0.02	2.62 ±0.01
24.18	0.00555	0.041	7.94 ±0.05	4.05 ±0.02	2.62 ±0.01
16.12	0.01875	0.062	7.34 ±0.03	4.01 ±0.02	2.61 ±0.01
8.06	0.15000	0.124	5.23 ±0.03	3.45 ±0.02	2.41 ±0.01
4.03	1.20000	0.248	2.25 ±0.01	1.81 ±0.01	1.72 ±0.01

Table 4.7: Data obtained for 150 monomers inside the box

L_b	Φ	L_b^{-1}	$\bar{R}_1$	$\bar{R}_3$	$\bar{R}_6$
48.36	0.00069	0.021	11.34 ±0.04	6.19 ±0.03	4.09 ±0.02
32.24	0.00234	0.03 1	11.02 ±0.05	6.21 ±0.04	4.06 ±0.02
24.18	0.00555	0.041	11.04 ±0.06	6.08 ±0.03	4.04 ±0.02
16.12	0.01875	0.062	9.70 ±0.05	5.88 ±0.03	3.95 ±0.02
8.06	0.15000	0.124	5.31 ±0.02	4.32 ±0.02	3.05 ±0.02
4.03	1.20000	0.248	2.41 ±0.01	1.76 ±0.01	1.54 ±0.01

Table 4.8: Data obtained for 300 monomers inside the box

ones found with the periodic box. In tables 4.5 4.6 4.7 4.8 are shown the data relative to the simulations.

4.0.2 Motion of the center of mass for a solution of rings

In this section we are going to briefly describe the MSD of the rings center of mass inside the shrinking sphere. The procedure is the same as the one adopted for a single ring in Chapter (3). However we do not have a large statistical sample due to the huge computational cost and we do not aim at computing the diffusion coefficient (which according to Rouse shoulb be $\sim D/N$), but we are interested in estimating the brownian time of the dynamics, for a purpose that will be clear in the next chapter. We computed Δ^2 for for systems of three and six rings in two cases : $N = 150$ and $N = 300$ total number of monomers; finding, as expected, that system with three rings have a bigger brownian time t_B than the system with six rings. As example we report in figure 4.7 and 4.8, the curves of Δ^2 respectively for a system with three rings and a system with six rings, both with $N = 300$. Notice that with $R_s = 5$ and R_S, the volume is too small for the rings to travel, by diffusion, a distance equal to their own raiuds of gyration. We do not report the plots for the other cases because they give the same exact informations.

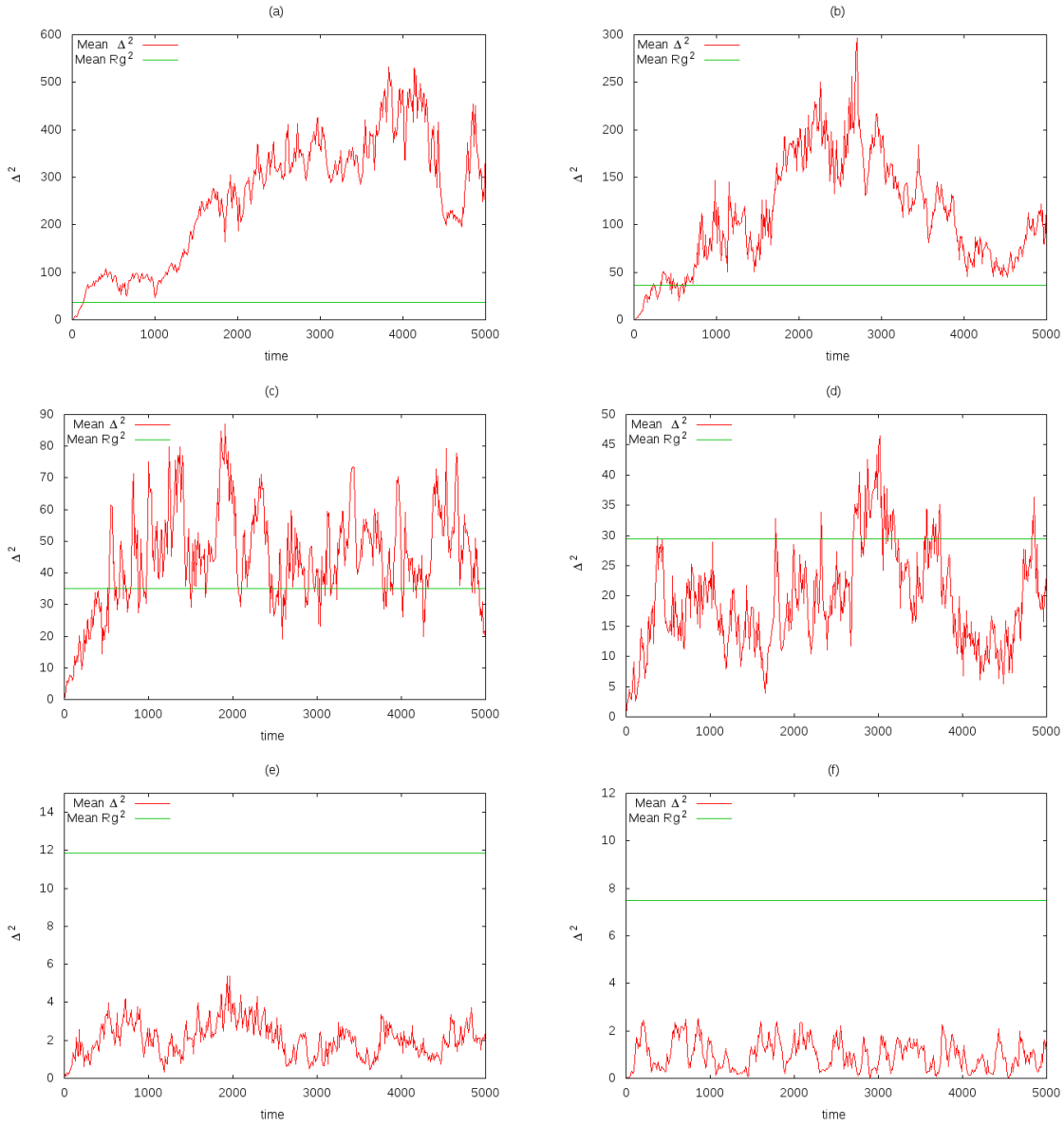

Figure 4.8: These plots show Δ^2 for a system with three rings and $N = 300$, inside a sphere with different radii ($R_S = 30, 20, 15, 10, 5, 2.5$). Each curve is the mean of Δ^2 of all three rings, since they are totally equivalent.

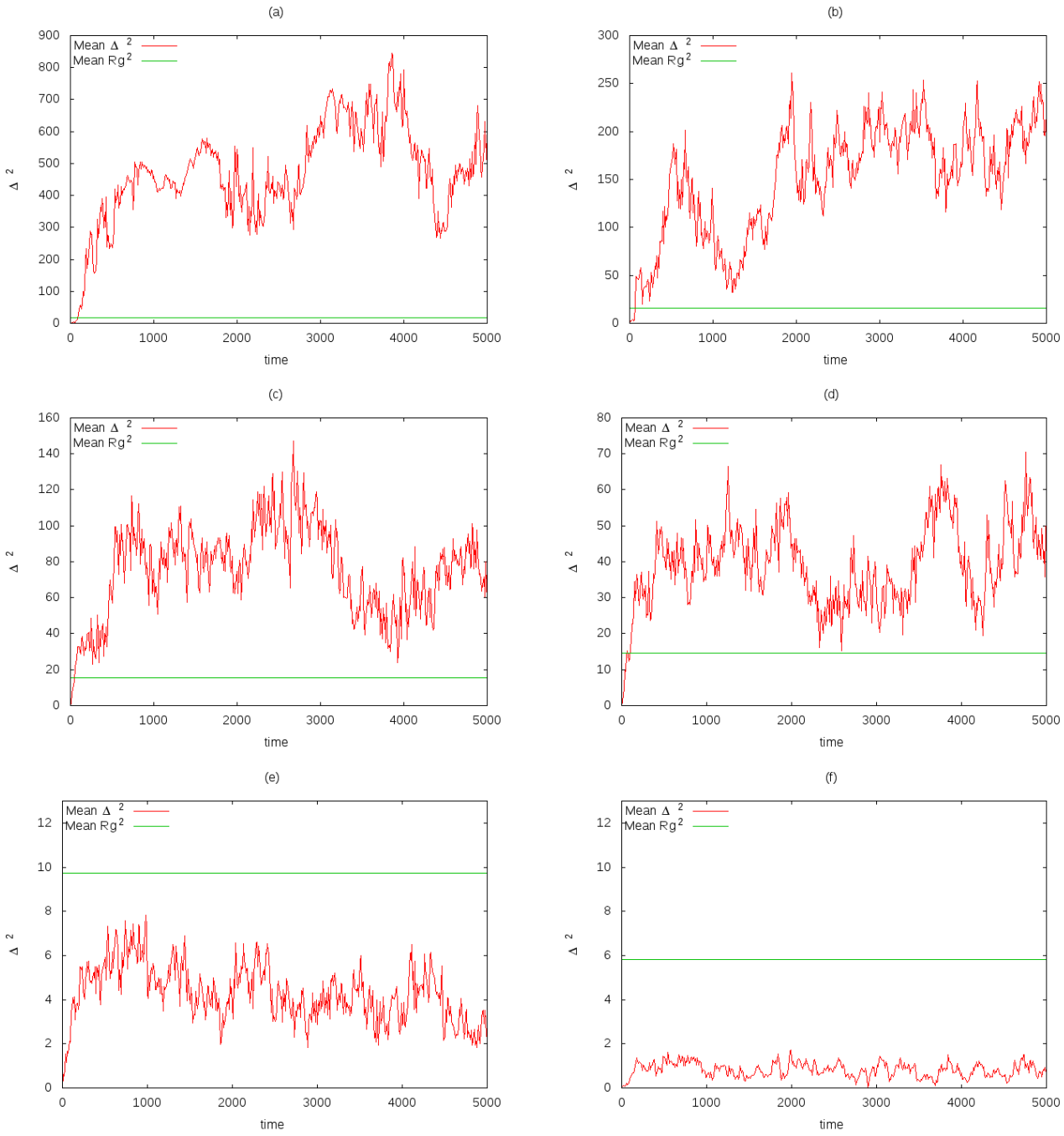

Figure 4.9: Plots of Δ^2 for the system with six rings and $N = 300$, inside a sphere with different radii ($R_S = 30, 20, 15, 10, 5, 2.5$). Each curve is the mean of Δ^2 of all six rings.

Chapter 5

Living Polymers

In this chapter we want to study how the possibility of swapping bonds affects an ensable of polymer rings. In particular we want to describe the distribution of the polymer length and verify if it converges to a steady-state, finding the relation between coefficients linked to the breakage and recombination rate.

5.1 Mean field theory of polymer recombination

The starting point of our analysis is the study conducted by M.E. Cates on living polymer chains. In Cates' model it is assumed that a chain can break with a fixed probability per unit time per unit lenght anywhere along its lenght. It is further assumed that the reverse reaction rate is proportional to the product of the concentration of the two reacting subchains and, moreover, that the rate constant is independent of the molecular weights of these two subchains. It is also assumed that successive breakage and recombination events regarding a given chain are uncorrelated. With these assumption, the equation governing the time development of the number density $n(N)dN$ of chains of lenght $N \pm \frac{1}{2}dN$ is :

$$\begin{aligned}\dot{n}(N) = &- c_1 N n(N) - c_2 n(N) \int_0^\infty dN' n(N') + 2c_1 \int_N^\infty dN' n(N') \\ &+ c_2 \int_0^\infty \int_0^\infty dN' dN'' n(N') n(N'') \delta(N' + N'' - N)\end{aligned} \tag{5.1}$$

Here the first represents the decrease in $N(L)$ by breakage, the second is the deacrease by reaction of chains of lenght L with others to form longer chains, the third is the reate of creating by breakage of longer chains, and the last is the rate of creation by fusion of two shorter chains to form one if lenght L. The parameters c_1 and c_2 are rate costant for breakage and recombination processes, respectively.
This equation admits a steady-state ($\dot{n} = 0$) solution:

$$n(N) = 2\frac{c_1}{c_2} exp\left(-\frac{N}{\bar{N}}\right) \tag{5.2}$$

where $\bar{N}$ depends on the overall polymer concentration $\rho = \int_0^\infty N n(N) dN$ as follows :

$$2\bar{N}^2 = \rho \frac{c_1}{c_2} \tag{5.3}$$

We aim to find out if equation 5.2 holds for an ensamble of living polymer rings, which can lead to the study of a stationary state. In order to perform such task we need to describe which factors contribute to the brakage and recombination processes and find appropriate rate coefficient like c_1 amd c_2.

5.2 Model and numerical implementation

5.2.1 Swap rules

In this section we describe how the simulation is build in order to represent the recombination of our system of rings. First of all we have to define the rules that govern the swap between bonds. In particular we have to explicit a cutoff distance at which swapping will be considered, in distance unit, and a time interval τ_{sw} during which , in average, a bond swap is attempted. Thus time scale τ_{sw} is linked to the number of step necessary during a simulation by the relation $N_{sw} = \tau_{sw} dt$, where dt is the timestep of the simulation. Moreover, the swap follows Monte Carlo rules using the Boltmann acceptance criterion. This mean that the probability of a bond swap between the i-th and j-the monomers is linked to the total energy difference of the system, before and after the swap [10]. If the energy decreases due to the swap operation, the bond swap is accepted. If the energy increases it is accepted with probability

$$P_{swap}(i \leftrightarrow j) \propto e^{-\beta \Delta E} \tag{5.4}$$

where ΔE difference includes changes in pairwise, bond, and angle energies. Whether the swap is accepted or rejected, no other swaps are attempted by this processor on this timestep.

5.2.2 Simulation parameters

As mentioned in the previous section, we need to define the cutoff distance and Nswap. In our simulation we set the cutoff distance $R_0 = 1.7$, which means that two monomers have to be close to interact, but not in contact with each other.
Regarding Nswap, the choiche is less immediate. In fact we want to stat the swapping after the system reaches an equilibrium, which means that the recombination time, computed as $\tau_s w = dt N_{sw}$ has to be bigger than the brownian time τ_B. In order to satisfy this condition, and with reference to the plots in figure 4.8 and 4.7 , we decided to work with the systems with six rings, total number of monomers $N_M = 150$ and $N_M = 300$, final radius of the sphere $R_S = 15$ and $R_S = 10$. In fact, thanks to the low value of the brownian time, we can choose a value such as $N_{sw} = 2000$, which derives from $\tau_{sw} = 2\tau_B$. In order to have a more efficient statistical sample we are also going to introduce a system with six rings, but $N_M = 450$.
This value of Nswap assures a satisfying number of swaps, enough to permorf a study like the one described in the introduction of this chapter.

5.3 Analysis and Results

In this section we are going to describe the evolution of the system, in order to find and describe a lenght distribution. In fact, according to Cates, the distribution of the number of rings at a fixed lenght follows an exponential behaviour. In particular we sample the data at four different

N	c_1 c_2	$\bar{N}$	N_{av}
150	8.81 ± 2.98	1.58 ± 0.25	8.5 ± 4.5
300	10.69 ± 1.48	1.96 ± 0.15	15.7 ± 2.13
450	14.46 ± 2.71	1.64 ± 0.14	24.4 ± 3.6

Table 5.1: Numerical results of our analysis, where we indicate with N_{av} the average length of the rings in the solution.

istants, in order to see how the distribution of the rings lenght changer over time. Every results that we show in this section is the average over ten different independent simulation.
As seen in section (5.1), the description of the stationary state depends on the density of polymers. Since we are going to describe the evolution of the system by means of discrete distribution, we have to redefine the polymers concentration as

$$\rho = \frac{\sum_{i=1}^{k} N_i n_i(N)}{\sum_{i=1}^{k} n_i(N)} \tag{5.5}$$

where

$$\bar{n_R} = \sum_{i=1}^{k} n_i(N) \tag{5.6}$$

is used as a normalization factor. During the data analysis we noticed that there are no major differences between the histograms at $R_S = 10$ and $R_S = 15$, because the volume difference is not big enough to be relevant. Using this fact to our advantage, we can improve the statistics of the data pool by taking the mean of the histograms at different R_S.
In figures 5.1, 5.2 and 5.3 we show the devolopment of the number density $n(N)$ over time for the three cases taken in exam (six rings and $N_M = 150, 300, 450$). As predicted by Cates, the number density seems to converge to a stationary state that can be described by the relation (5.2). This allows us, by means of an exponential fit, to compute $\bar{N}$ and the ratio between the rate constant for recombination and breakage: $\frac{c_1}{c_2}$. In figure 5.4 is possible to see the results of the exponeltial fit.
In figures 5.5 and 5.6 we show examples of the system's configuration at $t = 5000$.

In table (5.1) we report the numerical results of our analysis. The important resulst is that the rate costant for breakage, c_1, is considerably bigger than the one for recombination, c_2. In fact, as it is possible to see from the histograms in figures 5.1, 5.2 and 5.3, longer rings tend to decompose in favour of the ones with $3 \leq N_M \leq 10$ (three is the shorter length possible, because we need at least three bonds to form a ring). Secondly, the ratio c_1/c_2 grows with the total number of monomers, which means that is more probable for a long ring to break than to absorb a smaller one.

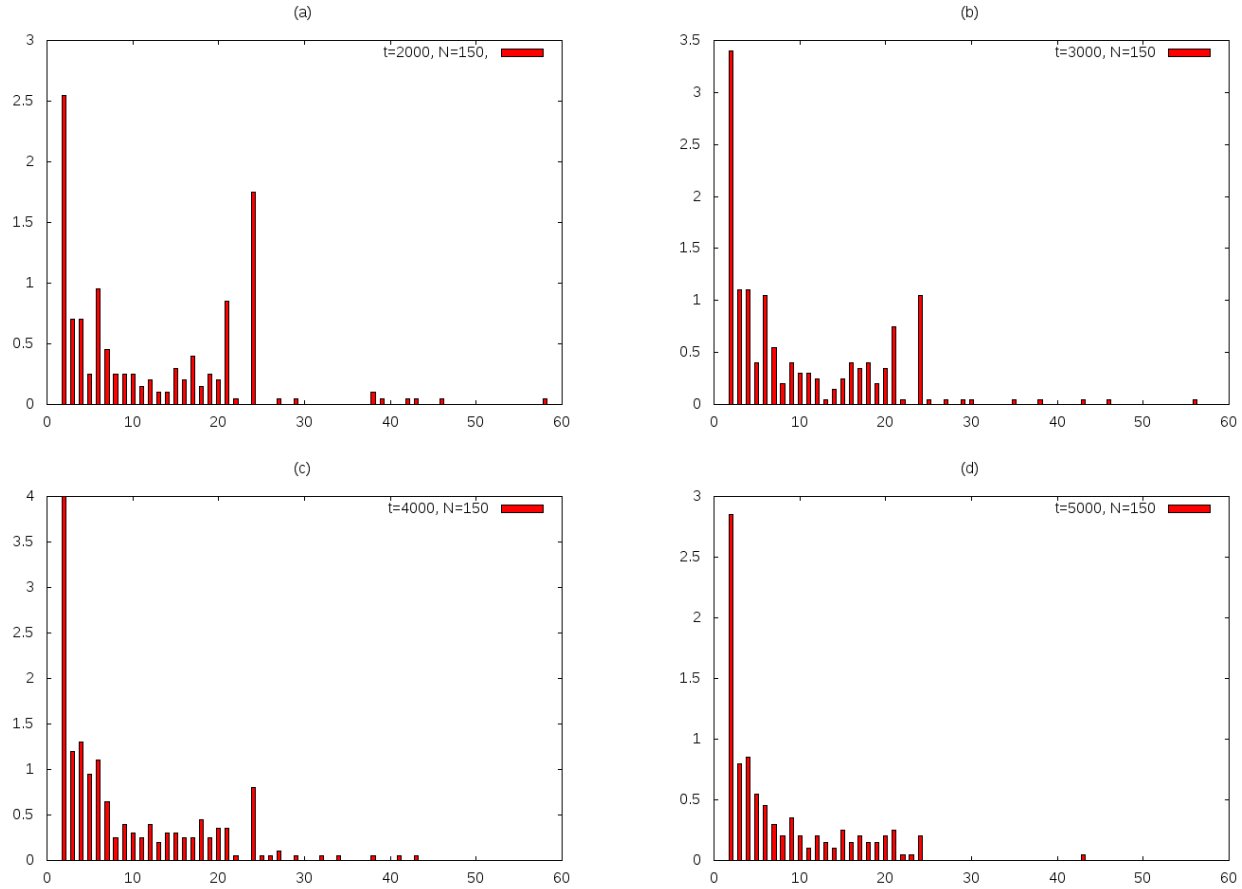

Figure 5.1: Time devolpment of the number density $n(N)$ for N=150 total number of monomers. We show how the system reaches its final configuration at $t = 5000$, sampling the data also at $t = 2000, 3000, 4000$. Notice that the distribution at $t = 5000$ seems to converge to an exponential behaviour, like the one shwon in formula (5.2).

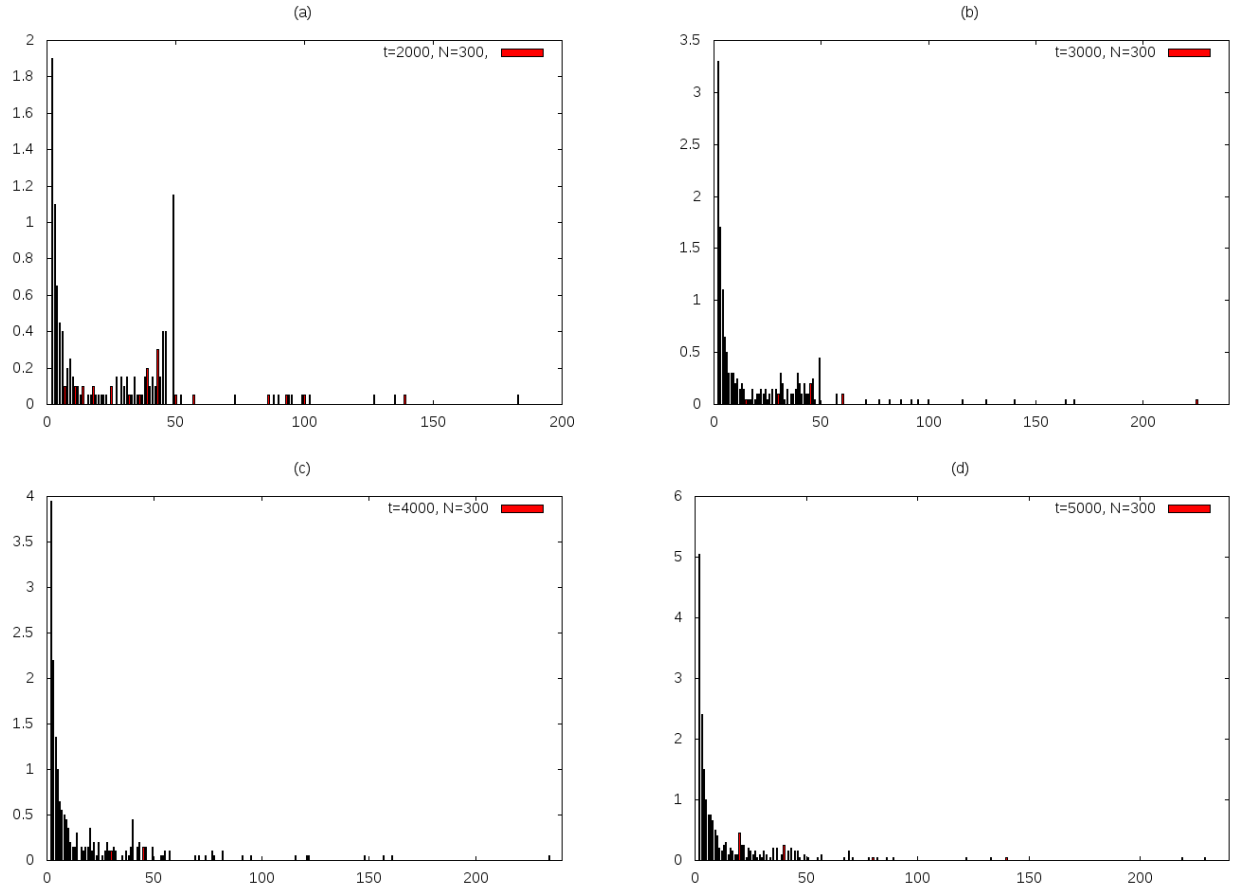

Figure 5.2: Time devolpment of the number density $n(N)$ for N=300 total number of monomers. We show how the system reaches its final configuration at $t = 5000$, sampling the data also at $t = 2000, 3000, 4000$. Similarly to the case $N_M = 150$, the distribution converges to an exponential behavior.

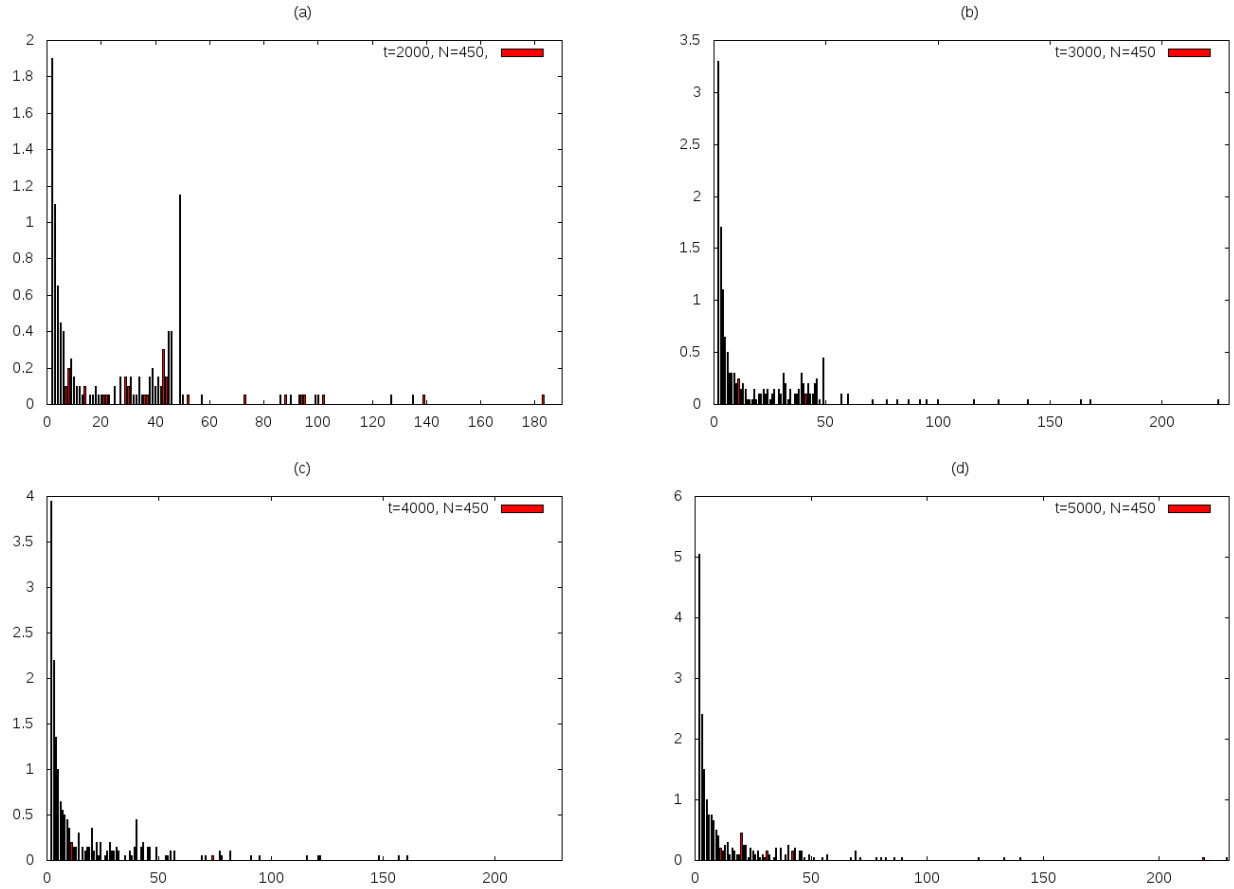

Figure 5.3: Time devolpment of the number density $n(N)$ for N=450 total number of monomers. We show how the system reaches its final configuration at $t = 5000$, sampling the data also at $t = 2000, 3000, 4000$. Again,like the cases $N_M = 150$ and $N_M = 300$, the distribution converges to an exponential behavior.

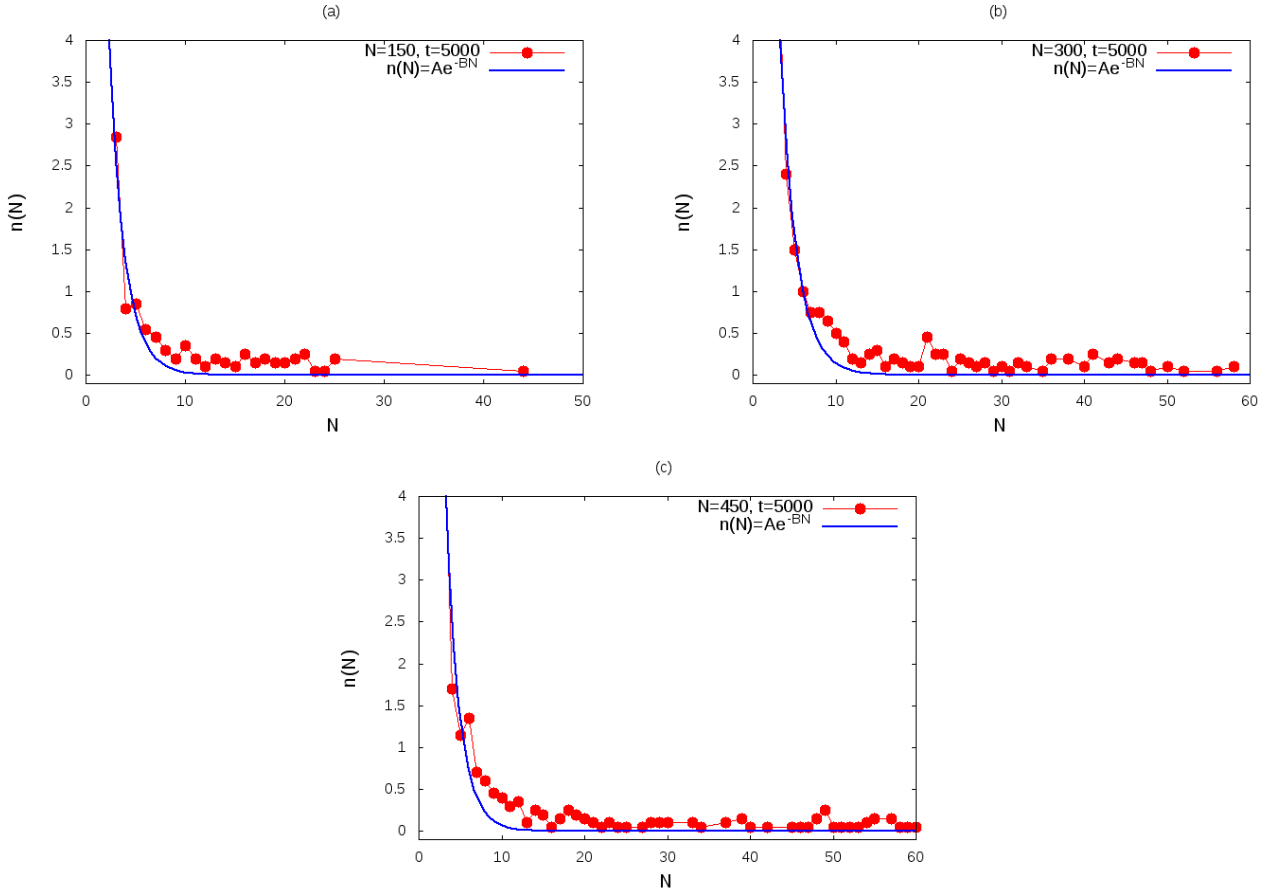

Figure 5.4: Exponentail fit of the number density $n(N)$ at $t = 5000$ for $N_M = 150$ (figure (a)), $N_M = 300$ (figure (b)), $N_M = 450$ (figure (c)). The blue line plots the function $n(N) = Ae^{-BN}$, where the coefficients A and B are numerically computed fitting the red points. In particular for $N_M = 150$ $A = 17.6 \pm 5.9$, $B = 0.63 \pm 0.11$; for $N_M = 300$ $A = 21.3 \pm 3.1$, $B = 0.50 \pm 0.03$; for $N_M = 450$ $A = 28.9 \pm 5.4$, $B = 0.61 \pm 0.05$

Figure 5.5: Example of a final configuration for a system with N=150. Remember that, even if it is not plotted, the rings are inside a sphere. It is possible to see that the presence of short ring is predominant. Notice that short rings tend to diffuse apart from the longer ones, minimizing the possibility of recombination.

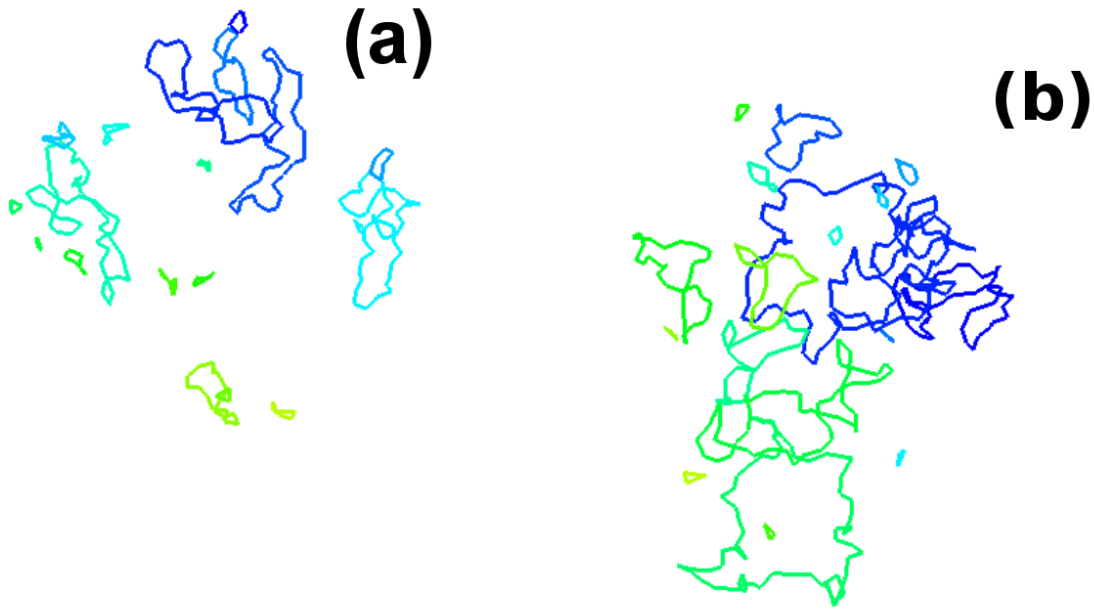

Figure 5.6: Example of a final configuration for a system with N=300 (figure (a)) and N=450 (figure (b)). This representation seems to be at odds with what we explained in the text: longer rings tend to decompose in favour of the smaller ones. However notice that the longer rings are far from the small ones (the swap takes place when the distance betweens two monomers is equal or less of 1.7), with no chance to interact. Moreover, long rings are very compacted, which means that there can be a bond swap between monomers of the same ring, leading to a breakage, since $c_1 > c_2$; hence, if we run a longer simulation ($t \gg 5000$), we expect to find a conformation similar to the one in figure 5.5.

Chapter 6

Conclusions

In this work we aimed at describing the behaviour of polymer rings under different cirumstances. We started by illustrating how these polymers are built: we introducend two different types of potential, Lennard-Jones and FENE, describing the connectivity between monomers and how introducing the constraint of self-avoidance. The introduction of the Lennard-Jones potential made possible the introduction of rescaled physical units, which we used throughout all the work .Then we describid the enveironment surrounding these polymers: we suppose that the polymer rings are in contact with a thermostat, which models an interaction with a background implicit solvent, at a given temperature T; this kind of backgroung leads to the presence of stachastic force. Once the potential were introduced, togheter with the stochastic component, was possible to integrate the equation of motion deriving from them by means of a velocity-Verlet method.
The integration of the equations of motion gave us the possibility to compute the radius of gyration of a ring, leading to information regarding its topology, and the mean square dispacement of its center of mass position, describing the diffusive nature of the dynamics. Firstly we focused our attention on systems with a single isolated ring inside an infinite volume, in different cases, changing the total number of monomers, i.e. the polymer's length. We then verified the scaling growth of the radius of gyration $R_g \sim N^{\nu}$, where ν is called the Flory exponent; then we tried to find a similar law for the relaxation time, however we worked with polymers too short to obatin satisfying results, in fact this relation holds for large values of N.
Successively we described the effect of confinement on a single ring in two case, N=150 and N=300. To model the confinment we put the ring inside a shrinking spherical volume. We described the surface of the sphere as a bounding wall, which interacts with the nearby particles by mens of the 9/3 potential. We found ou that the rings lose the typical dependence $R_g \sim N^{\nu}$ when the radius of the sphere, R_s satisfies $1/R_S \leq 0.1$. After computing the radius of gyration, we diverted our attention to the mortion of the rings' center of mass, computing the brownian time of the dynamics (τ_B) and the diffusion coefficient. We discovered that the brownian time is heavely linked with the polymer lenght, it is smaller for shorter rings, while under confinment the ring is unable to travel a distance equal to its raidus of gyration, so that the dynamics starts to lose its diffusive nature. This behaviour reflects in the value of the diffusion coefficient, which is significantly smaller when $1/R_S \leq 0.1$.
Afterwards we described the confinement of solutions of several rings in two different-shaped volumes: sphere with hard wall and periodic cubic box. We confronted systems with the same number of monomers, but dirrent number of rings. In particular we studied cases with two

different total number of monomers, N=150 and N=300, and three different number of rings, $N_R = 1$, $N_R = 3$, $N_R = 6$. We firstly characterized the radius of gyration for every case, discovering that rings with differnt lengths tend to reach the same limit value of the radius. Then we tried to study the dynamic of the center of mass. However, due to the great computational cost, we were only able to obtain information on the brownian time: for systems of six rings is almost immediate, while for system of three rings $200 \leq \tau_B \leq 1000$, depending on the size of the volume.
Lastly we described the behaviour of living polymer rings. We had firsty to described under which condition a polymer is able to break and recombined, then we exposed the carachteristic of our simulations : swap rules and which type of system we analysied. We decided to start from a solution with six rings, because of the low brownian time, which gave us the possibility of choosing a small swap time, and hence an accessible total run time. We were able to describe the convergence or the lenght distrubution of the polymers to an exponential-like steady state, leady to the computation of the ratio between the rate costant for breakage and recombination. We discovered that the system tend to a conformation where the breakage coefficient is several times bigger than the recombination one, and presence of small rings is predominant.

Appendices

Appendix A

Example of LAMMPS script

```
###
# Reference paper:
# K. Kremer and G. S. Grest
# Dynamics of entangled linear polymer melts: A molecular-dynamics simulation
# J Chem Phys 92, 5057 (1990)
###
###

# Box and units (use LJ units and period boundaries)
###
units lj

# atom_style bond # no stiffness

atom_style angle # with stiffness
boundary ff ff ff

###

# Pair interactions require lists of neighbours to be calculated
###
neighbor 0.3 bin
# neighbor 1.0 bin
neigh_modify every 1 delay 1 check yes
### Generate RESTART file, SPECIAL format, not a .txt file ###

### Useful if simulation crashes ###
# restart 1000 rings_3.restart
##############################
# processors 2 1 1

### READ "start" data file ###

# read_data lammps_input_nr10_nb50
read_data rings.dat
```

```
#######################
variable d index swap_15_1 swap_15_2 swap_15_3 swap_15_4 swap_15_5 swap_15_6

swap_15_7 swap_15_8 swap_15_9 swap_15_10
variable s index 17177 17277 17377 17477 18000 14000 19999 155555 19325 17000
variable l index 2000 3000 4000 5000 5463 2145 3215 6846 6541 2909
shell cd $d

### READ "REstart" data file ###

# read_restart rings_3.restart_1000000
#######################
### reset timestep ###

reset_timestep 0
#######################
###

# Define groups (atom type 1 is group 'all')
###
group ring1 type 1
group ring2 type 2
group ring3 type 3


    # group microrheology molecule 10
###

# Dump configs - "simple dumpings"
###
# dump 1 all custom 10000 rings_3.dump x y z ix iy iz
# dump_modify 1 format "
    ###
# Dump configs + box coords
###
dump 1 all custom 10000 rings_3_eq.dump.* id x y z ix iy iz
dump_modify 1 format "# dump id all atom 10000 dump.rings_3
dump id all custom 1000 dump.rings_3_eq id type x y z ix iy iz
# dump d2 all image 10000 img-*.ppm type type bond none 2.5 zoom 15
compute 1 all property/local batom1 batom2 btype

compute 2 all bond/local dist eng
dump 3 all local 1000 dump.rings_bonds_3_eq index c_1[1] c_1[2] c_1[3] c_2[1] c_2[2]
#######################################################################

# Stiffness term
#
# E = K * (1+cos(theta)), K>0
```

```
#
angle_style cosine
# angle_coeff 1 5.0 OK swap
# angle_coeff 1 20.0
angle_coeff 1 1.0
##############################################################################
##############################################################################

# Pair interaction between non-bonded atoms
#
# Lennard-Jones 12-6 potential with cutoff:
# potential E=4epsilon[ (sigma/r)^12 - (sigma/r)^6] for r<r_cut
#
# 1.12246 = 2^(1/6) is the minimum of the potential
pair_style lj/cut 1.12246152962189

# pair_style lj/cut 1.58
#

# pair_modify shift yes adds a constant to the potential such
# that E(r_cut)=0. Forces remains unchanged.
#
pair_modify shift yes

#

# pair_coeff for lj/cut, specify 4:
# * atom type interacting with
# * atom type
# * epsilon (energy units)
# * sigma (distance units)
#
pair_coeff * * 1.0 1.0

##############################################################################

    ##########################################################################
# Pair interaction between non-bonded atoms
#
# soft potential, for PUSHING apart overlapping atoms
# potential E=A*(1 + cos(pi*r/r_c))
#
# 1.12246 = 2^(1/6) is the cut-off r_c
# pair_style soft 1.12246152962189

#

# pair_coeff for soft, specify 4:
```

```
# * atom type interacting with
# * atom type
# * A_start
# * A_stop
#
# pair_coeff 1 1 4.0 100.0

##############################################################
##############################################################

# Pair interaction between bonded atoms
#
# Fene potential + Lennard Jones 12-6:
#
# E= - 0.5 K R0^2 ln[ 1- (r/R0)^2]
# + 4epsilon[ (sigma/r)^12 - (sigma/r)^6] + epsilon
#
bond_style fene

#

# For style fene, specify:
# * bond type
# * K (energy/distance^2)
# * R0 (distance)
# * epsilon (energy) (LJ component)
# * sigma (distance) (LJ component)
#
# bond_coeff 1 30.0 8.0 1.0 1.0

# bond_coeff 1 30.0 1.5 1.0 1.0
bond_coeff 1 10.0 1.8 1.0 1.0
special_bonds fene #<=== I M P O R T A N T (new command)

##############################################

    ##########################################
# Pair interaction between bonded atoms
#
# Harmonic potential:
#
# E= K * (R-R0)^2
#
# bond_style harmonic

#

# For style harmonic, specify:
```

```
# * bond type
# * K (energy/distance^2)
# * R0 (distance)
#
# bond_coeff 1 60.0 1.0

##############################################################
region mySphere sphere 0.0 0.0 0.0 100 side in units box



    variable r0 equal 68.0
variable rf equal 10.0
variable rate equal 0.1
variable ratek equal 0.1
variable r equal ramp(v_r0,v_rf)
variable rad equal "gyration(all)"

variable time equal "step*dt"
variable kappa equal "0.001 + step*dt*v_ratek"
###

# Set up fixes
###
fix 1 all nve ### NVE ensemble

fix 2 all langevin 1.0 1.0 2.0 $s ###Langevin integrator Tstart Tstop 1/friction rndseed
fix 3 all indent 10 sphere 0.0 0.0 0.0 v_r side in units box
# fix 4 all bond/swap 1 0.5 1.7 2717
# fix 3 all wall/region mySphere lj93 1.0 1.0 1.122
# fix pull microrheology addforce 0 0 0


    ##### Sample thermodynamic info (temperature, energy, pressure, etc.) #####
# thermo 500
# thermo_style custom step temp epair emol press pxx pyy pzz vol v_r
##############################################################


    ###
# set timestep of integrator
###
timestep 0.001 #0.012 #0.002


###
# run integration for a number of steps
##
```

```
    compute R1e ring1 gyration
compute R2e ring2 gyration
compute R3e ring3 gyration
variable RG1e equal c_R1e

variable RG2e equal c_R2e
variable RG3e equal c_R3e


    fix extra all print 100 "$time $RG1e $RG2e $RG3e " file RG_lam_eq.dat screen no


    run 500000
reset_timestep 0

unfix 3

unfix extra
undump 1
undump id
undump 3


    fix 3 all indent 10 sphere 0.0 0.0 0.0 v_rf side in units box
fix 4 all bond/swap 100000 0.5 1.7 $l
dump 1 all custom 100000 rings_3.dump.* id x y z ix iy iz

dump id all custom 10000 dump.rings_3 id type x y z ix iy iz
dump 3 all local 10000 dump.rings_bonds_3 index c_1[1] c_1[2] c_1[3] c_2[1] c_2[2]
compute R1 ring1 gyration

compute R2 ring2 gyration
compute R3 ring3 gyration
variable RG1 equal c_R1

variable RG2 equal c_R2
variable RG3 equal c_R3
fix extra all print 10000 "$time $RG1 $RG2 $RG3 " file RG_lam.dat screen no

thermo 5000

thermo_style custom step temp epair emol press pxx pyy pzz vol v_r
run 5000000

shell cd ..
clear
next d
next s
next l
```

```
jump polymer_sfera_15.lam
# "print 'Polymer: Rg = $rad;'"
```

Bibliography

[1] M. Rubinstein and R. Colby, *Polymer Physics*, Oxford University Press, Oxford, 2003.

[2] M.E. Cates, *Macromolecules*, 1987,**20**, 2289-2296.

[3] C. Micheletti, D.Marenduzzo, E.Orlandini, *Polymers with spatial or topological constraints: Theoretical and computational results*, Physics Reports, 2011, 1-73

[4] C. Micheletti, D.Marenduzzo, E.Orlandini, D.W. Sumners,*Topological friction strongly affects viral DNA ejection*, PNAS, 2013, **110(50)**:20081-20086.

[5] D.W. Heermann, *Theoretical Biophysics*, Universitat Heidelberg, 2006.

[6] D.C Rapaport, *The Art of Molecular Dynamics Simulation*, Cambridge University Press, Cambridge, 1995.

[7] P. Poier, P. Bacova, A.J. Moreno, C.N. Likos, R. Blaak, *Anisotropic effective interactions and stack formation in mixtures of semiflexible ring polymers*, Soft Matter, 2016, **12**, 4805-4820.

[8] Prince E. Rouse, *A Theory of the Linear Viscoelastic Properties of Dilute Solutions of Coiling Polymers*, J. Chem. Phys. 21, 1272 (1953).

[9] J. Des Cloizeaux, J. Phys., 1981, 42, 635–652.

[10] N. Metropolis, A.W. Rosenbluth, M.N. Rosenbluth. A.H. Teller and E. Teller, *Equation of State Calculations by Fast Computing Machines* J. Chem. Phys. 21 (1953) 1087-1092.